Assessing the Influence of Complex Terrain on Severe Convective Environments in Northeastern Alabama

BRANDEN KATONA[a] AND PAUL MARKOWSKI[a]

[a] *The Pennsylvania State University, University Park, Pennsylvania*

(Manuscript received 4 August 2020, in final form 10 March 2021)

ABSTRACT: Storms crossing complex terrain can potentially encounter rapidly changing convective environments. However, our understanding of terrain-induced variability in convective storm environments remains limited. HRRR data are used to create climatologies of popular convective storm forecasting parameters for different wind regimes. Self-organizing maps (SOMs) are used to generate six different low-level wind regimes, characterized by different wind directions, for which popular instability and vertical wind shear parameters are averaged. The climatologies show that both instability and vertical wind shear are highly variable in regions of complex terrain, and that the spatial distributions of perturbations relative to the terrain are dependent on the low-level wind direction. Idealized simulations are used to investigate the origins of some of the perturbations seen in the SOM climatologies. The idealized simulations replicate many of the features in the SOM climatologies, which facilitates analysis of their dynamical origins. Terrain influences are greatest when winds are approximately perpendicular to the terrain. In such cases, a standing wave can develop in the lee, leading to an increase in low-level wind speed and a reduction in vertical wind shear with the valley lee of the plateau. Additionally, CAPE tends to be decreased and LCL heights are increased in the lee of the terrain where relative humidity within the boundary layer is locally decreased.

SIGNIFICANCE STATEMENT: This work investigates how the environments associated with severe storms vary around a plateau in northeastern Alabama. We use operational high-resolution model output and idealized simulations to determine which parameters used to forecast severe storms are most affected by terrain, where the parameters tend to be increased or decreased relative to the terrain, and why such increases and decreases occur. These parameters that characterize the likelihood of severe thunderstorms and tornado formation are all affected by the terrain, primarily when the wind has a strong perpendicular component relative to the long axis of the terrain. It is not clear that these changes would tend to make storms consistently more or less strong near the terrain.

KEYWORDS: Complex terrain; Severe storms; Storm environments

1. Introduction

Convective storms frequently cross complex terrain and may encounter highly variable convective environments. These varying environments make short-term forecasting of storm intensity and storm hazards difficult, in part because many of these variations are smaller in scale than most current numerical weather prediction models can resolve. Improving the conceptual model for how convective environments vary in regions of complex terrain and understanding when terrain-induced changes are most likely to occur are important for the anticipation of rapid changes in convective storm intensity.

Spatial variation in convective storm frequency near complex terrain is associated with terrain-induced changes to storm environments. Radar climatologies have shown that local maxima and minima in convective storm frequency are often aligned with local terrain features (Murray and Colle 2011; Kirshbaum et al. 2016; Kovacs and Kirshbaum 2016). Storms tended to occur most frequently in regions where terrain-modified flow resulted in reduced convective inhibition (CIN) and/or increased convective available potential energy (CAPE; Kirshbaum et al. 2016; Kovacs and Kirshbaum 2016). While these climatologies link storm frequency to changes in the near-storm environment, they fail to say how terrain might affect storm severity.

Observations of convective storms in regions of complex terrain show that these storms can intensify quickly when encountering a more favorable storm environment. In addition to terrain modifying a storm's cold pool, which can affect squall line propagation (e.g., Teng et al. 2000; Frame and Markowski 2006; Reeves and Lin 2007; Letkewicz and Parker 2010, 2011), storms also realize terrain-induced changes to local instability and wind shear profiles that can result in changes to updraft and mesocyclone strength. Terrain-modified winds may contribute to strengthening and backing of near-surface flow, which can locally increase low-level wind shear and streamwise vorticity available to storms (Hannesen et al. 1998; LaPenta et al. 2005; Bosart et al. 2006; Schneider 2009; Tang et al. 2016). Additionally, the increase in low-level wind speed may enhance moisture flux, resulting in locally increased CAPE (Bosart et al. 2006; Tang et al. 2016). An analysis of tornadic and severe nontornadic storms in New York state showed that the tornadic storms generally did not produce tornadoes until encountering favorable environments in the Mohawk

Katona's current affiliation: NOAA/OAR/National Severe Storms Laboratory, Norman, Oklahoma.

Corresponding author: Branden Katona, katona@psu.edu

DOI: 10.1175/WAF-D-20-0136.1

and Hudson River valleys (Wunsch and French 2020). These observations point to an important role that complex terrain can play in the modification of convective storm severity.

Simulations of supercell storms show that terrain-induced perturbations to CAPE and CIN may be important for modifying supercell updraft and mesocyclone strength. Unlike observations, idealized simulations allow a researcher to understand how a storm evolves in initially identical environments both in the absence and presence of terrain. Markowski and Dotzek (2011) noted that CAPE was generally greater on the upstream (relative to the low-level wind direction) side of an infinitely long ridge, while CIN was increased on the downstream side. Storm mesocyclones and updrafts of supercells in these idealized simulations generally weakened where the storms encountered increased CIN (Markowski and Dotzek 2011). As both observed and modeled storms generally appear to respond to these terrain-induced environmental perturbations, it is important to understand where such perturbations occur and under what conditions they are most likely.

Recent work has used both numerical forecast data and observations to examine where terrain-induced changes to convective environments occur. Katona et al. (2016) used data from the High-Resolution Rapid Refresh (HRRR; Smith et al. 2008; Benjamin et al. 2016) model to create climatologies of convective environments in the Northeast and Southeast. The locations of maxima and minima of these parameters were analyzed relative to local terrain features. CAPE was lowest over regions of higher topography, the distribution of 0–1-km storm-relative helicity (SRH01) maxima relative to terrain was strongly influenced by wind direction, and the significant tornado parameter (STP) was primarily maximized in coastal regions and locations just west of the Mississippi River. The regional focus of Katona et al. (2016) was insufficient to determine how convective environments may vary locally around smaller-scale terrain features. Tornadogenesis may be more likely as storms encounter some of these smaller-scale features (Lyza and Knupp 2018). This increase in tornado likelihood near a plateau system in northeastern Alabama was attributed to enhanced low-level wind shear atop the plateau associated with modifications to the low-level flow on days where flow is largely perpendicular to the plateau's long axis (Lyza et al. 2020). It is not known how frequently these terrain-induced modifications occur and what their effects on storms are.

The southern end of the Appalachian Mountains is characterized by a hill and valley system with a southwest-to-northeast orientation. Observations from the VORTEX-Southeast (VORTEX-SE) project show variations in cloud base height and low-level wind shear near the plateaus and valleys in this region (Lyza et al. 2020). It is not clear how frequently these terrain-induced changes in convective environments occur, how the changes relate to low-level flow direction, and what the physical mechanisms behind many of these changes are. Observations from Lyza and Knupp (2018) and Lyza et al. (2020) suggest the mountain Froude number may be important. Complex terrain is important in modifying local convective environments, and understanding when and where such modifications occur can help forecasters anticipate potential storm intensification.

In this article, we investigate the influence of local terrain features in the Southeast on heterogeneity in storm environments using climatologies and idealized simulations to identify where and when such terrain-induced changes to the convective environment are most likely. The focus is on northeastern Alabama given the interest in the possibility of severe weather being influenced by terrain in this particular area (e.g., Lyza and Knupp 2018; Bryan et al. 2018). This area has also been a region of targeted observations in the VORTEX-Southeast project. Given the recent interest in this particular terrain feature and its focus as a part of a field campaign, we extend some of our past work (Katona et al. 2016) to investigate under which conditions terrain is most likely to modify local near-storm environments and where these perturbations tend to occur relative to the terrain features. This work answers the following questions:

1) Where in northeastern Alabama are terrain-induced perturbations most likely?
2) How does low-level wind direction influence where these perturbations occur?
3) What are the physical origins of the most common perturbations?

Section 2 details the methodology used to create the climatologies of convective environments and presents the results of these climatologies. Section 3 details the setup used in the numerical simulations used to explore the physical origins of the perturbations discussed in section 2. The results from the simulations are also discussed in section 3 and compared to the results of the climatologies. A discussion of the results and conclusions are presented in section 4.

2. HRRR climatologies

a. Methods

High-resolution operational numerical weather prediction model output is used to identify where complex terrain modifies near-storm environments. The initial approach follows that of Katona et al. (2016), and the reader is directed to their study for a more thorough review of the dataset and methods. A long-term average of convective environments on days supportive of convective storms is generated. Such an approach mitigates the influence of day-to-day synoptic and mesoscale variability on the spatial patterns of convective environments. The HRRR is used for the climatologies, as it was in Katona et al. (2016). The HRRR is well suited for the purpose of exploring near-storm environments in regions of complex terrain because it has relatively fine grid spacing (3 km) and forecasts are generated hourly using a cycled data assimilation system. The HRRR should be able to resolve wavelengths on the order of 15–20 km given its grid spacing, which is sufficient to resolve some of the mesoscale effects of topography on the surrounding environments. Although the HRRR has not had the exact same model configuration over the time period used, the changes did not produce noticeable impacts on the climatologies (not shown).

Climatologies are created using 2-h HRRR forecasts of convective parameters, which are valid at 2100 UTC (1600–1700 local

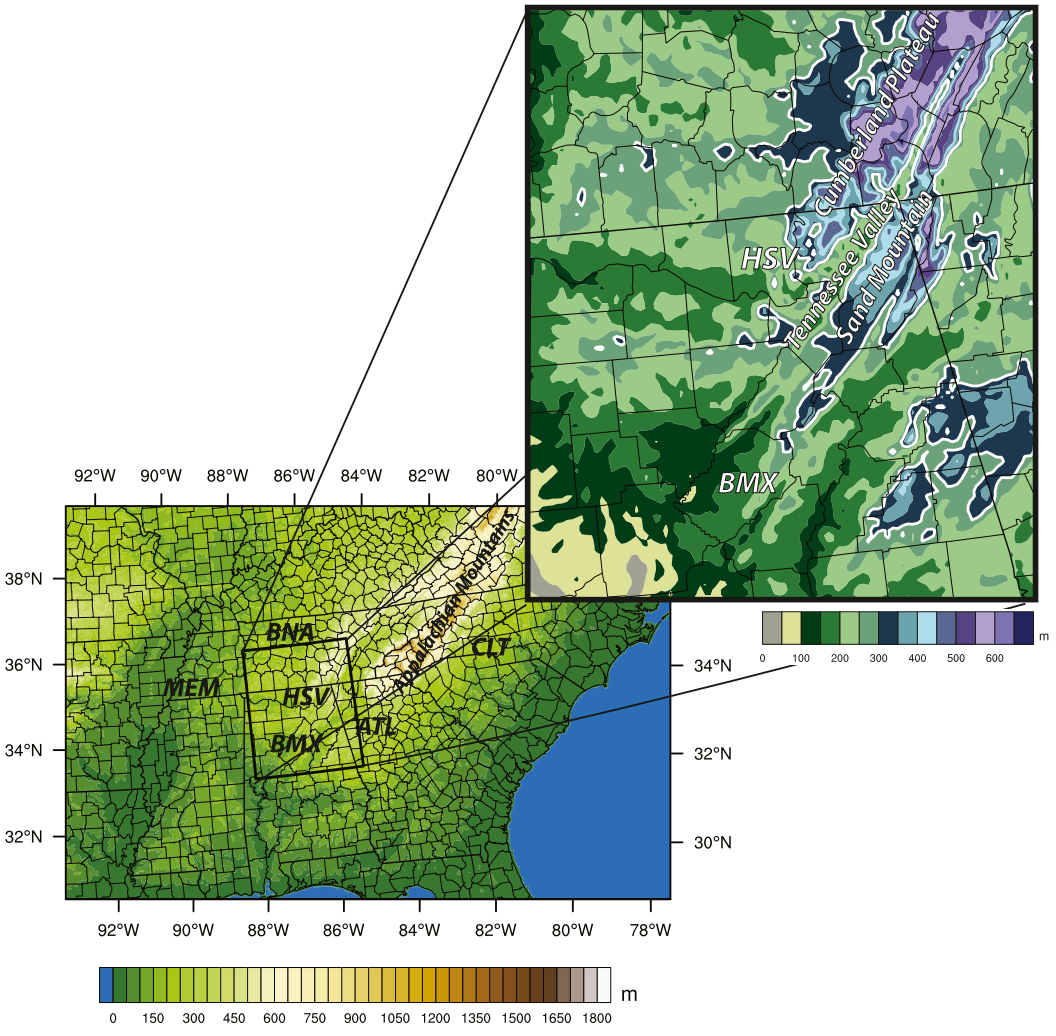

FIG. 1. Elevation in the domain used in the HRRR climatology and SOM analysis. Some large cities throughout the domain are labeled with three letter airport codes for reference. The black box and zoomed-in image show the area of focus for the SOM analysis. The white line in the inset figure is the 300-m isoheight line. Terrain features and large cities are labeled for reference.

time) and 0600 UTC (0100–0200 local time), for days between 1 February and 30 September from 2013 through 2018. Averaging 2-h forecasts instead of the 0-h forecast minimizes the influence of biased surface observations on the climatologies and "ensures physical consistency within the three-dimensional model dynamics and parameterizations" (Katona et al. 2016). This approach reduces the appearance of seemingly unphysical patterns that were initially present in long-term climatologies of the 0-h forecasts (not shown). Only days for which convective storms might be possible in the analysis domain are included in the climatologies. "Convective days" are defined as those days on which mean-layer CAPE (MLCAPE; calculated using the average equivalent potential temperature of the three lowest 30-hPa layers) exceeds 500 J kg^{-1} over at least 10% of land-based grid points. This calculation is performed on the large-analysis domain that makes up the broader southeastern region (Fig. 1). Using this larger domain for the convective day determination allows for consistency with prior work (Katona et al. 2016). Additionally, using only the small area in northern Alabama greatly reduces the number of available days available to use in these climatologies. Reducing the number of convective days limits the representativeness of the conclusions drawn from the climatologies. The climatologies are relatively insensitive to the definition of a convective day; using all days between 1 February and 30 September for the years used here reduces the magnitude of the values seen in the climatologies, but does not change the spatial patterns of relative maxima and minima (not shown). This approach may miss some convective events, but the qualitative patterns demonstrated below should remain unchanged unless one is only focused on high-shear, low-CAPE regimes (e.g., Sherburn and Parker 2014). All grid points on a given convective day are included in the averages.

Parameters commonly used when forecasting severe convective storms are averaged on convective days to create the

climatologies. CAPE is a necessary but insufficient condition for the formation of severe convective storms and has little useful predictive skill in the forecasting of tornadoes (Thompson et al. 2003). In this study, we use MLCAPE computed using a parcel defined by the average equivalent potential temperature of the three lowest 30-hPa layers above the surface. Mean-layer convective inhibition (MLCIN) is the integral of the negative buoyancy between the initial parcel level and the level of free convection. CIN represents the amount of work required to lift a parcel to its level of free convection. In general, large amounts of CIN are detrimental to the initiation and maintenance of convective storms. A forecast parameter frequently used by forecasters to assess supercell and tornado potential is storm-relative helicity (SRH). SRH is the vertically integrated product of the storm-relative winds and the environmental vorticity vector. Increasing amounts of storm-relative helicity are generally indicative of the potential of a stronger low-level mesocyclone that is able to contract near-surface vertical vorticity into tornado strength (Markowski and Richardson 2014; Coffer and Parker 2017). SRH between the surface and 1 km (SRH01) has been shown to be a good discriminator between nontornadic supercells and those capable of producing strong tornadoes (Thompson et al. 2003). SRH is sensitive to changes in the near-surface wind field, and modifications in the near-surface flow field produced by topography may induce large changes in SRH. The SRH01 calculated in the HRRR uses the Bunkers et al. (2000) storm motion estimate. The STP (Thompson et al. 2003) is a linear combination of CAPE, SRH01, lifted condensation level (LCL) heights, and 0–6-km vertical wind shear that has been shown to discriminate well between environments capable of producing strong tornadoes versus those that do not produce tornadoes. STP values exceeding 1 tend to be associated with supercells capable of producing tornadoes (Thompson et al. 2003). These parameters are not the only ones that may be affected by terrain, but they are commonly used by many forecasters on days where severe convective storms are possible.

The influence of near-surface flow direction is important in determining where parameters are perturbed relative to terrain features. While supercell dynamics depend solely on the storm-relative wind field (Markowski and Richardson 2006), terrain-relative wind fields determine where convective environments are perturbed. Past work has shown near-surface flow direction can have a large impact on which regions in complex terrain are relative maxima or minima (Katona et al. 2016). Flow direction is important for determining where standing waves occur and where flow may be susceptible to flow channeling. Since wind direction is so important in determining the influence of terrain, it makes sense to sort the convective days into different groups characterized by similar near-surface wind directions.

We generate climatologies for different near-surface wind directions using self-organizing maps. Self-organizing maps (SOMs) are a form of unsupervised neural networks in which a user-defined number of characteristic patterns are derived from the input vectors (Kohonen 2013). The procedure used here is similar to the one used in other severe weather climatologies that have used SOMs (Nowotarski and Jensen 2013; Anderson-Frey et al. 2017). The input vectors to the SOM are 2-h forecasts of perturbation mean sea level pressure (MSLP), valid at 2100 and 0600 UTC. MSLP perturbations are calculated by subtracting the mean MSLP from the MSLP forecast in the Southeast domain (Fig. 1). Using perturbation MSLP rather than full MSLP creates more distinct low-level flow patterns between nodes. Six nodes are initialized in a two row by three column configuration using random input vectors derived from the distribution of all input data with number n vectors. With over 850 convective days in the dataset, using six nodes easily satisfies the rule of thumb that each node should contain, on average, at least 50 cases (Kohonen 2013). Creating more nodes does not result in a more meaningful clustering of the convective days and may reduce generality (not shown). Each of the n input vectors is randomly drawn and then compared to the six nodes. The vector is assigned to the node which it most closely resembles by selecting the node with which it has the smallest Euclidean distance. After being matched to a node, that node is updated to more closely resemble the input vector. In addition to updating the best matching node, surrounding nodes are also updated using an inverse exponential weighting function so that they are not nudged to resemble the input vector as closely. Each of the n input vectors is randomly drawn and used to update the nodes of the SOM. This process is repeated 200 times with the input vectors drawn in differing random orders each time until the patterns observed in the nodes stabilize.

Once the six nodes are created, each of the convective days is sorted into the node that it most closely resembles. Then, the average MLCAPE, MLCIN, SRH01, and STP are calculated for each convective day in the node, along with the mean 10-m wind vectors. While the MSLP patterns over the entire Southeast (Fig. 1) are used to create the nodes, the mean convective parameters are plotted over northeastern Alabama, where topography likely modifies the local convective environment (Katona et al. 2016; Lyza and Knupp 2018; Lyza et al. 2020). The mean spatial distributions of local maxima and minima of convective environments are analyzed relative to the complex topography that characterizes this part of the Southeast. The intent of these climatologies is to demonstrate where convective environments are most susceptible to modification by terrain in northeastern Alabama, while acknowledging that the full magnitude of the modification on any given day is likely not represented here. As such, the reader is cautioned that CAPE, CIN, SRH, and STP values on any given convective day will likely have different magnitudes than presented herein.

b. Results

The Southeast is characterized by a variety of geographic features. Coastal plains near the Gulf of Mexico and regions surrounding the Mississippi River are generally flat. Areas farther from the coast gently slope upward until encountering the Appalachian Mountains in northeastern Alabama and northern Georgia (Fig. 1). For several years, terrain-induced modifications of severe storm environments have been a focus of VORTEX-SE. Terrain in this region is characterized by the Cumberland Plateau and the Sand Mountain Plateau, which sit several hundred meters above the Tennessee Valley. It is

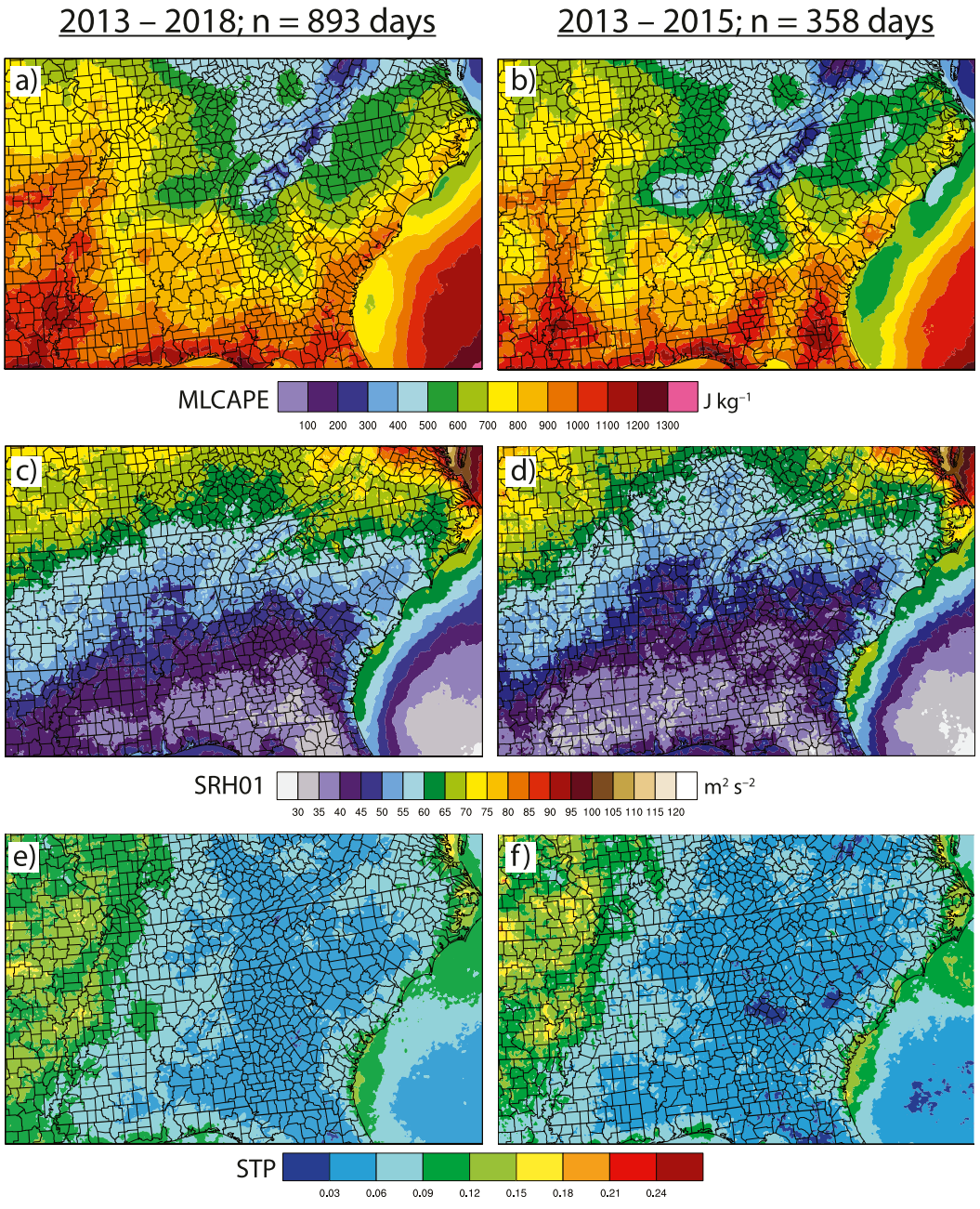

FIG. 2. (a) Mean MLCAPE on all convective days in the expanded dataset including the years 2013–18. (b) As in (a), but for the dataset used by Katona et al. (2016). (c),(d) As in (a) and (b), but for SRH01. (e),(f) As in (a) and (b), but for STP.

thought that this region may be a local tornado hot spot (Lyza and Knupp 2018). Both the HRRR climatologies discussed below and idealized modeling results presented in the following section will analyze where and how convective environments are modified by the terrain in northeastern Alabama.

1) HRRR CLIMATOLOGIES

The mean convective parameters are displayed in Fig. 2 are very similar in both magnitude and spatial distribution when compared to those from Katona et al. (2016). This indicates that the addition of another 3 years of data does not qualitatively change the conclusions about how mean convective environments are distributed in regions of complex topography. Although the Katona et al. (2016) conclusions are unaffected, adding more convective days to the dataset allows for a larger number of groups to be created to better analyze how wind direction and static stability influence terrain's effects on convective environments.

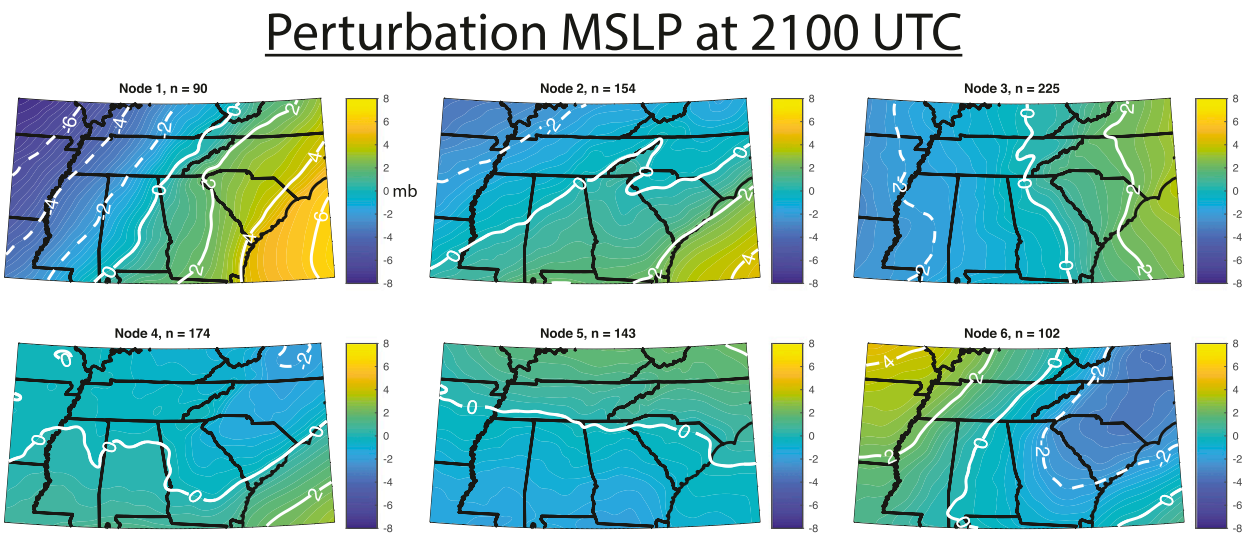

FIG. 3. Average perturbation mean sea level pressure (mb) on convective days sorted into each of the six SOM nodes, valid at 2100 UTC. White contours show the perturbation isobars and perturbation isobars are labeled every 2 mb in the positive (solid) and negative (dashed) directions.

The SOM analysis creates nodes characterized by distinct pressure patterns. The nodes show a wide variety of perturbation MSLP patterns commonly seen in the Southeast on days when convective storms may be possible (Fig. 3). Node 1 is characterized by an anomalously low MSLP in the northwest part of the analysis region, while node 6 is the most different from node 1 and is characterized by anomalously low pressure from South Carolina through Virginia (Fig. 3). The remaining nodes are characterized by generally weaker MSLP anomalies than those seen in nodes 1 and 6. Each node is characterized by different near-surface flow directions, ranging from out of the south (node 1) to out of the northwest (node 6). The near-surface flow impinges upon the local complex terrain features from a variety of different directions in the dataset, allowing for changes in where convective environments are perturbed relative to the terrain features.

Each node is analyzed for the frequency with which different severe hazards occur. Storm reports from the Storm Prediction Center's Severe Weather Database Files page (https://www.spc.noaa.gov/wcm/#data) are used to determine if any of the nodes is associated with a higher incidence of particular types of severe weather. The number of days containing tornado, severe wind, and severe hail reports in the small domain in northeastern Alabama and the fraction of days in each node containing one of these reports shows if any of the nodes are anomalously associated with a particular hazard (Fig. 4). Because one day may be associated with hundreds of severe reports, the number of days on which these hazards

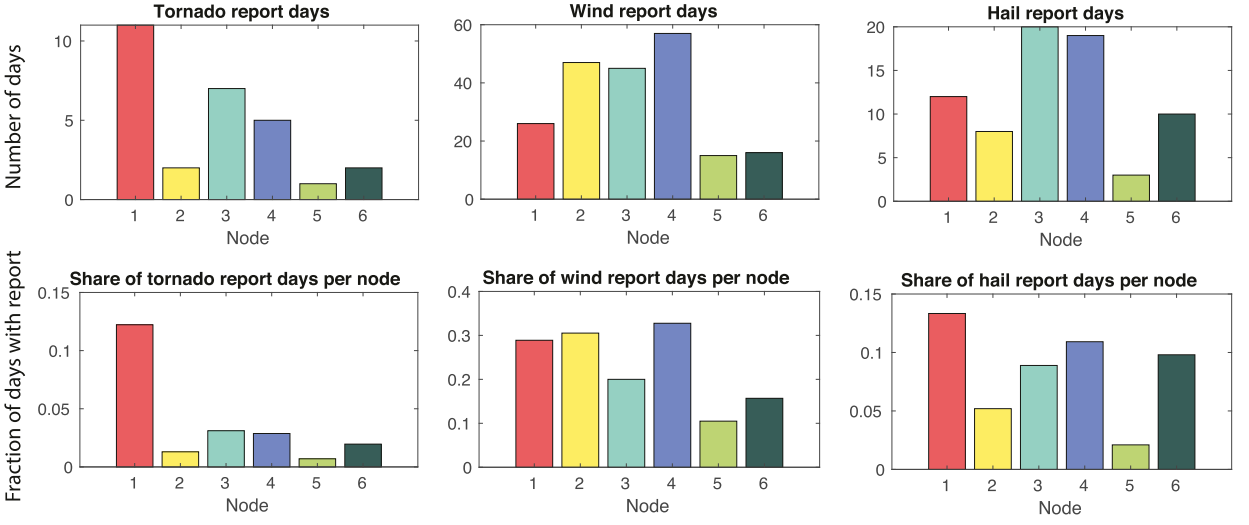

FIG. 4. (top) Number of convective days on which tornadoes, severe wind, and severe hail are reported within each node. (bottom) Percentage of convective days on which the hazard occurs within each node.

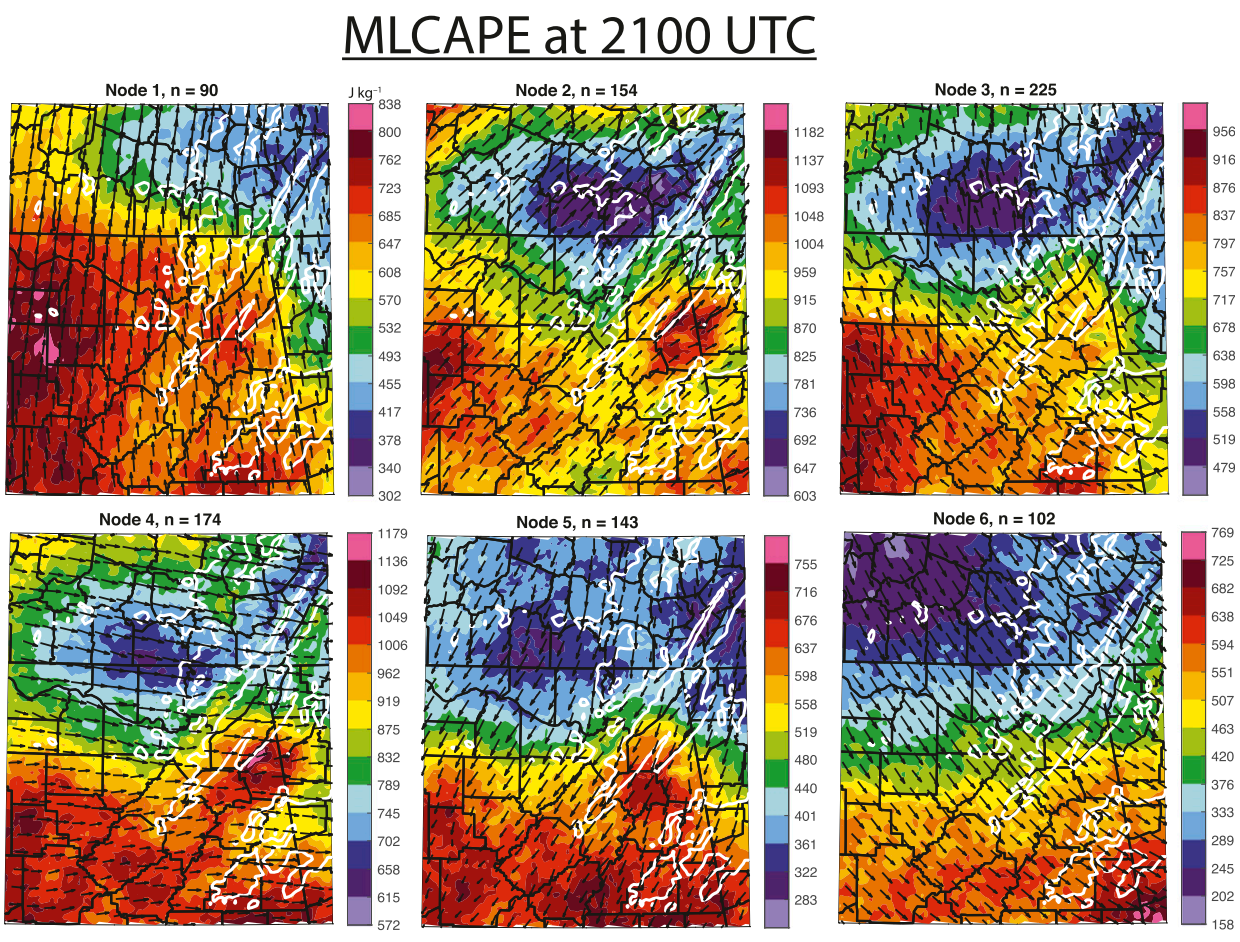

FIG. 5. Mean MLCAPE (J kg^{-1}) for convective days sorted into each node, valid at 2100 UTC. The vectors are the mean 10-m wind direction forecast at 2100 UTC on each of the convective days. The white line represents the 300-m isoheight line.

occur within each node is a more robust way of analyzing frequency of severe weather events. Node 1 contains the greatest number of tornado reports and the most frequent occurrence of days with tornado reports. It is likely that these tornado reports come from both supercells and quasi-linear convective systems (QLCSs). While the parameters discussed below are primarily used to assess supercell tornadogenesis, they also have some utility in forecasting QLCS tornadogenesis (Thompson et al. 2012). Severe wind is reported at a similar frequency in nodes 1, 2, and 4; severe hail is reported most frequently in node 1, while also occurring on about 10% of convective days sorted into nodes 3, 4, and 6.

2) DAYTIME CONVECTIVE ENVIRONMENTS IN REGIONS OF COMPLEX TERRAIN

MLCAPE tends to be less variable in regions of complex terrain compared to many of the other parameters examined here. Generally, MLCAPE exhibits a latitudinal decrease throughout the domain and lower MLCAPE is commonly found at higher elevations in eastern Tennessee. In node 1, it is not clear that MLCAPE is noticeably perturbed in the vicinity of the terrain system in northeastern Alabama (Fig. 5). Several other nodes suggest that, under some near-surface flow regimes, MLCAPE is slightly higher on top of the plateau and to the immediate southeast of the plateau than in surrounding areas (Fig. 5, nodes 2, 3, and 5). In these nodes, storms encountering the plateau from the west would experience larger MLCAPE as they ascend the plateau. The lack of perturbation to the MLCAPE fields could be due to the presence of well-mixed boundary layers on most convective days. In well-mixed boundary layers present on many convective days, parcel mean-layer properties would not vary much between the slightly higher terrain and the surrounding low-lying regions. The influence of terrain on MLCAPE near complex terrain in northeastern Alabama is uncertain, as there is a large amount of node-to-node variability.

MLCIN perturbations align much more closely with terrain gradients than MLCAPE (Fig. 6). MLCIN is also more variable in regions of complex terrain than MLCAPE. Small changes in CIN (owing to changes in mean-layer parcel properties) are likely more noticeable than those to CAPE, because the relative change in magnitude is generally greater for CIN than for CAPE. So, while there are likely days on which CIN changes little between the plateau and surrounding areas

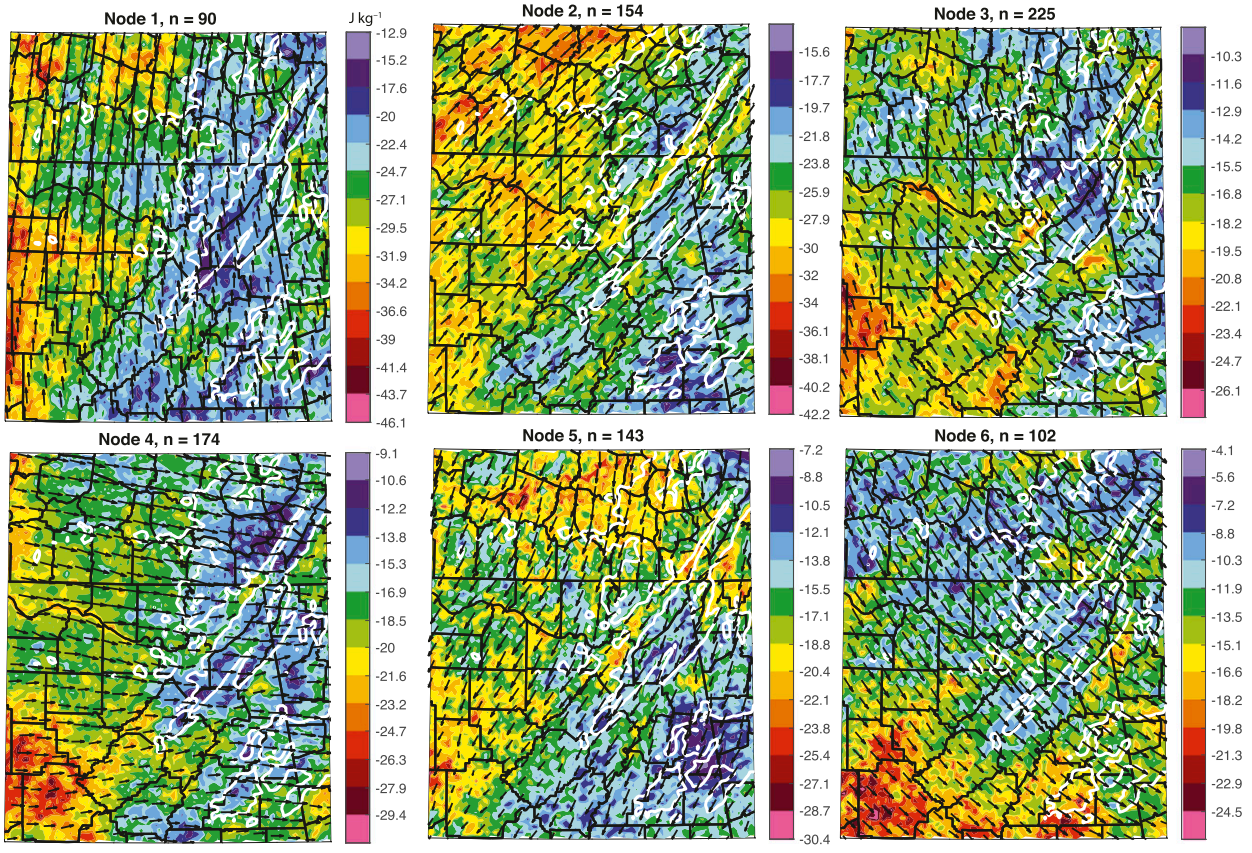

FIG. 6. As in Fig. 5, but for MLCIN (J kg^{-1}).

(such as days with well mixed boundary layers), the days on which there are drastic differences are the ones that are most highlighted in this climatology. MLCIN magnitude can be decreased by as much as 50% on top of the higher terrain, whereas MLCAPE tends to be increased by 10%–20%. In node 1, MLCIN is fairly uniform near the complex terrain, as the main pattern in the node is a westward increase in MLCIN (Fig. 6). In the remaining nodes, MLCIN magnitude tends to be lowest in regions of higher terrain across all nodes and higher in the Tennessee Valley and the flatter regions of north-central and northwestern Alabama and into southern Tennessee. In most nodes, MLCAPE is largest and MLCIN is lowest in regions that are about 200 m above surrounding areas.

It seems unlikely that terrain modification of flow is the reason for these differences. Decreases in CIN are generally seen at higher elevations where relative humidity becomes locally increased, either due to diurnally driven mountain circulations (e.g., Weckwerth et al. 2014; Panosetti et al. 2016) and when water vapor mixing ratio remains constant while potential temperature increases with height (Markowski and Dotzek 2011). It is likely that both mountain circulations and increasing potential temperature in the boundary layer affect the mean MLCIN fields seen in each node. Events occurring during the cooler portions of the analysis time period (February–April) may have boundary layers with ample low-level moisture and potential temperature increasing with height, which would lead to lower CIN at higher elevations. During the summer when diurnal heating is strong and boundary layer winds are weak, mountain circulations drive upslope flow (e.g., Banta 1990) and result in less negative CIN atop the plateau. Vertical profiles of potential temperature and the presence of diurnal mountain circulations likely both contribute to the pattern of MLCIN around the Cumberland and Sand Mountain Plateaus seen in the SOM climatologies.

SRH01 is particularly sensitive to changes in low-level flow speed and direction within the complex terrain system in northeastern Alabama. Node 1 contains the largest SRH01 values of all nodes (Fig. 7). SRH01 maxima occur over the higher regions of the Cumberland and Sand Mountain Plateaus along with the western edge of the analysis domain. A local minimum occurs primarily in the northern half of the Tennessee Valley, in addition to SRH01 being minimized in the southeastern portion of the domain. The variability in SRH01 is well portrayed in the idealized models and physical origins of these perturbations are discussed in a later section. In node 2, flow is primarily from the southwest and is largely parallel to the major axis of both plateaus. Mean wind vectors in the Tennessee Valley, where SRH01 is locally maximized, are backed relative to those in the

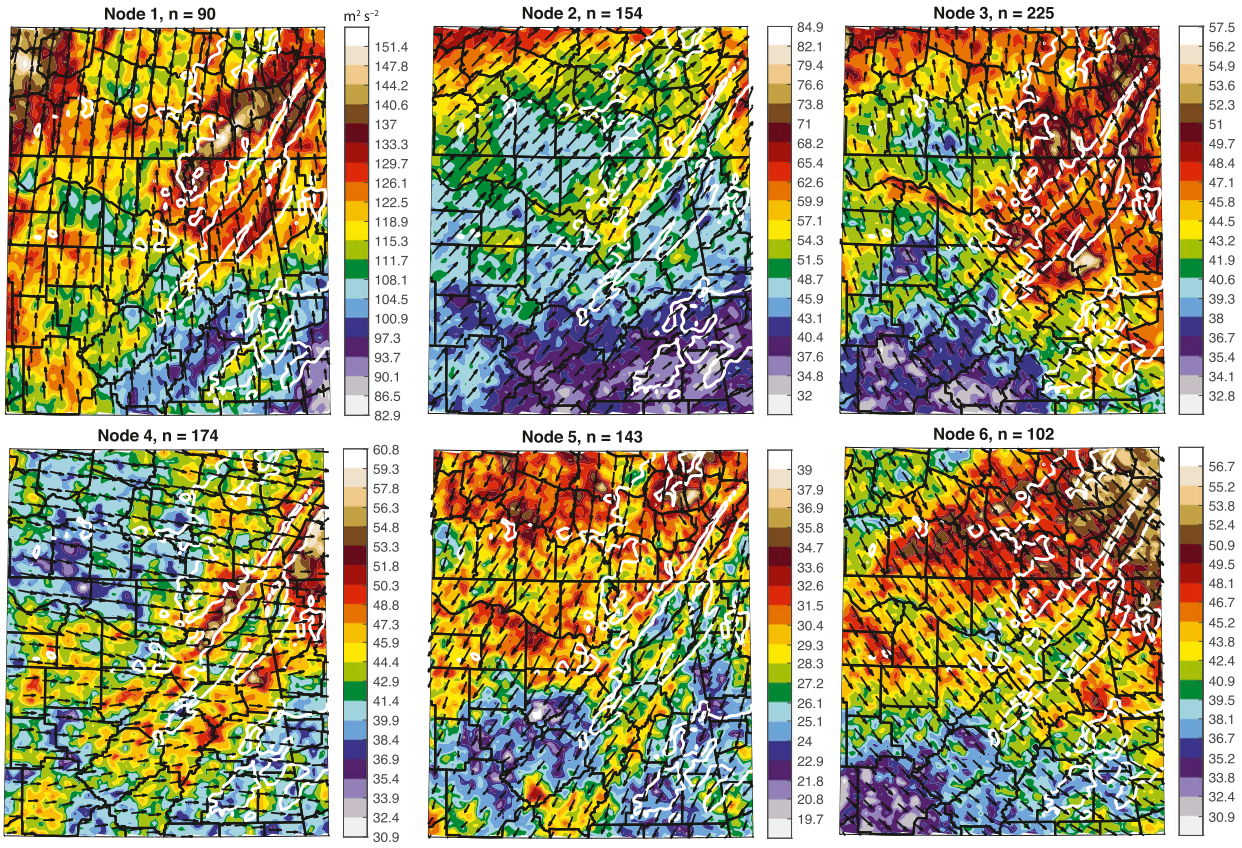

FIG. 7. As in Fig. 5, but for SRH01 ($m^2 s^{-2}$).

far field. This local backing of the winds likely increases low-level hodograph area and SRH01. Node 4 is characterized by westerly winds impinging upon Sand Mountain. SRH01 is maximized primarily at the base of the Sand Mountain Plateau while becoming a local minimum on the western edge (Fig. 7). The locations of certain maxima and minima change over relatively short distances and vary according the direction of the mean wind impinging on the northeastern Alabama terrain system.

Complex terrain can locally affect the STP. STP is a linear combination of two of the parameters already discussed, MLCAPE and SRH01, while also including LCL height and 0–6-km shear. SRH01 is highly variable in regions of complex terrain, and LCL height should be too given that changes in LCL height likely correlate with changes in terrain height. The mean values of STP in the climatologies are small because appreciable STP occurs relatively infrequently compared to the other parameters discussed above (Fig. 8). On days where STP indicates strong tornadoes are possible, the values will almost certainly be higher than those in the averages presented here. The reader is advised to use relative maxima and minima to identify where large STP values tend to occur most frequently. Node 1 has by far the greatest STP values (Fig. 8). This matches well with the propensity for this node to be associated with both the greatest number of tornado days and greatest fraction of days in the node that report tornadoes (Fig. 4). STP tends to be locally higher than surrounding regions on top of the Sand Mountain Plateau and southern portions of the Cumberland Plateau, as well as in western Alabama where the terrain is fairly flat. In node 2, which has the second highest STP values out of any node and southwesterly winds, there is little difference in STP between the Tennessee Valley and Sand Mountain or Cumberland plateaus (Fig. 8). STP is low in the remaining nodes, indicating infrequent occurrence of modest STP values within the node which makes analyzing perturbations in these nodes difficult. Under strong southerly flow, conditions are favorable for tornadoes throughout the domain, and these environments are locally most favorable on top of the plateaus in northeastern Alabama.

A breakdown of the terms comprising STP helps determine which of the four components is most affected by the terrain. The mean contributions from each parameter comprising STP are plotted in Fig. 9. The MLCAPE term is not higher on top of the plateau compared to surrounding locations at lower altitudes. The SRH01 contribution to STP is largest over the Cumberland Plateau and over the far northwestern portion of

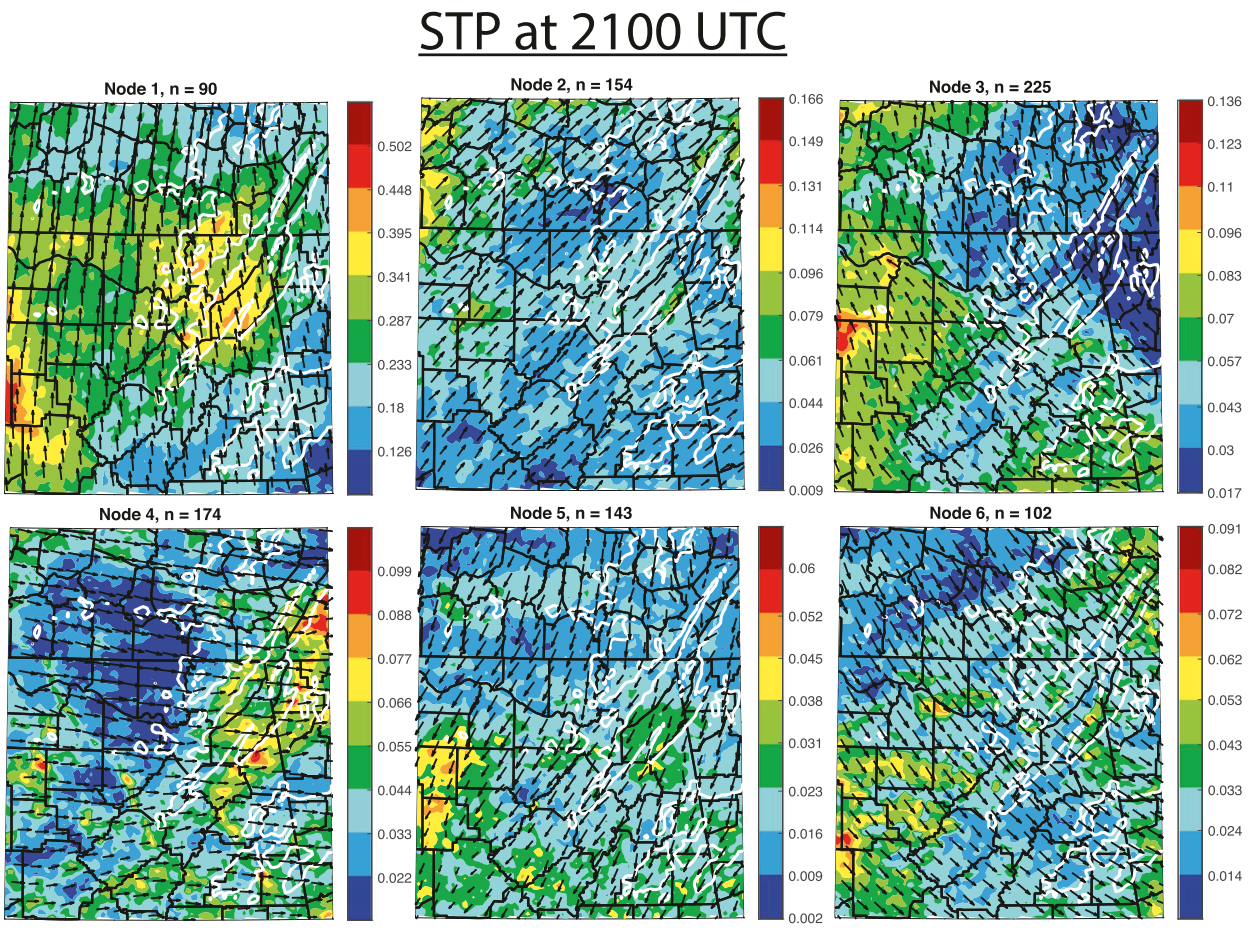

FIG. 8. As in Fig. 5, but for STP.

the domain. Low LCL heights also contribute to large STP values on the Cumberland and Sand Mountain Plateaus. LCL heights scale proportionally with terrain height; near-surface parcels in higher terrain would likely be closer to the level at which cloud bases form. Last, 0–6-km shear magnitude generally increases with latitude, but there may be a local increase over the Cumberland Plateau relative to this background latitudinal increase. Larger STP over Sand Mountain seems predominantly due to larger SRH01 and lower LCL heights. Spatial changes in SRH01 have been associated with tornadic and nontornadic supercells evolving in close proximity (Klees et al. 2016). Lower LCL heights are generally associated with tornadic supercells, but the influence of spatial variability in LCL height on tornadogenesis is not known. Although mean convective environments may be more favorable for strong tornadoes in the vicinity of the Sand Mountain Plateau, it is difficult to know what the effects of locally increased STP are on any given storm traversing this terrain system under background southerly flow.

3) NOCTURNAL CONVECTIVE ENVIRONMENTS IN REGIONS OF COMPLEX TERRAIN

The self-organizing map procedure is also performed for HRRR forecasts that are valid at 0600 UTC, corresponding to 0100–0200 local time. Because a relatively large proportion of tornadoes occur in nocturnal environments in the Southeast (Krocak and Brooks 2018), the influence of terrain on these environments is analyzed because they likely contain different boundary layer stability profiles and wind magnitudes than those occurring during the day. There are fewer convective days included for the nocturnal climatologies because fewer cases meet the convective day criteria. Despite the reduction in overall convective days, all nodes still meet the recommendation that the nodes contain at least 50 input vectors each (Kohonen 2013). The mean MSLP perturbation patterns are virtually identical to those shown in Fig. 3 (not shown). The wind speeds within the nocturnal nodes are weaker than in the diurnal nodes (e.g., Fig. 10). Winds generally weaken in the stable boundary layer at night as convective mixing ceases. The winds in nodes 1 and 6 best resemble their diurnal counterparts, and the prevailing winds in the remaining nodes are relatively weak. Because surface winds are weaker, the perturbations seen in the diurnal climatologies are not expected to be replicated here.

MLCAPE at night, unlike in the diurnal climatologies, has a somewhat strong relationship to local terrain features. In node 1, MLCAPE is slightly larger atop Sand Mountain than in the Tennessee Valley, but this decrease in MLCAPE is fairly

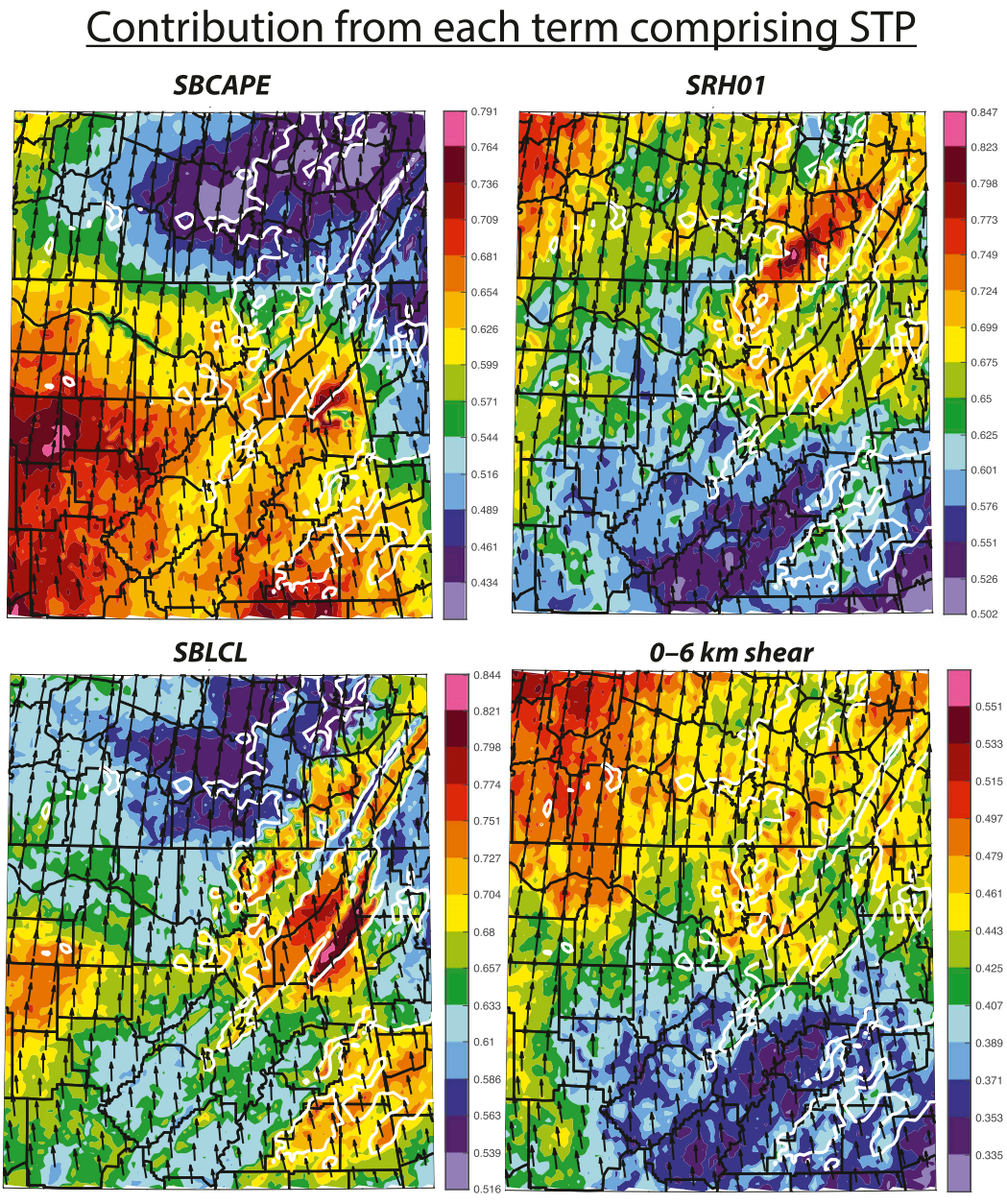

FIG. 9. Mean values of each STP term on convective days sorted into node 1.

consistent with the general latitudinal decrease present in this node (Fig. 10). Nodes 2, 3, 4, and 5 all have higher mean MLCAPE values in the Tennessee Valley compared to the surrounding higher terrain (Fig. 10). These MLCAPE perturbations are well aligned with the local terrain features, likely indicating characteristics of the mixed layer parcels from regions of higher terrain are different than those at surrounding lower regions. CAPE is generally weaker at night, so changes in CAPE in regions of complex terrain may be important in the evolution of nocturnal convective events.

Nocturnal MLCIN varies greatly in regions of complex terrain like it does during the day. MLCIN is stronger at night than during the day. In most nodes, MLCIN is weaker on top of the higher terrain than in the surrounding lower areas (Fig. 11). Nocturnal inversions in the boundary layer lead to parcels originating at lower altitudes having to do more work to overcome the increased stability than those originating atop the terrain. Parcels from higher altitudes have their mixed layer properties composed of air that more closely matches the characteristics of the most unstable parcels in the column. The question remains, however, if nocturnal storms have the propensity to intensify as they ascend to higher terrain and begin to ingest parcels with less MLCIN and more MLCAPE compared to surrounding areas.

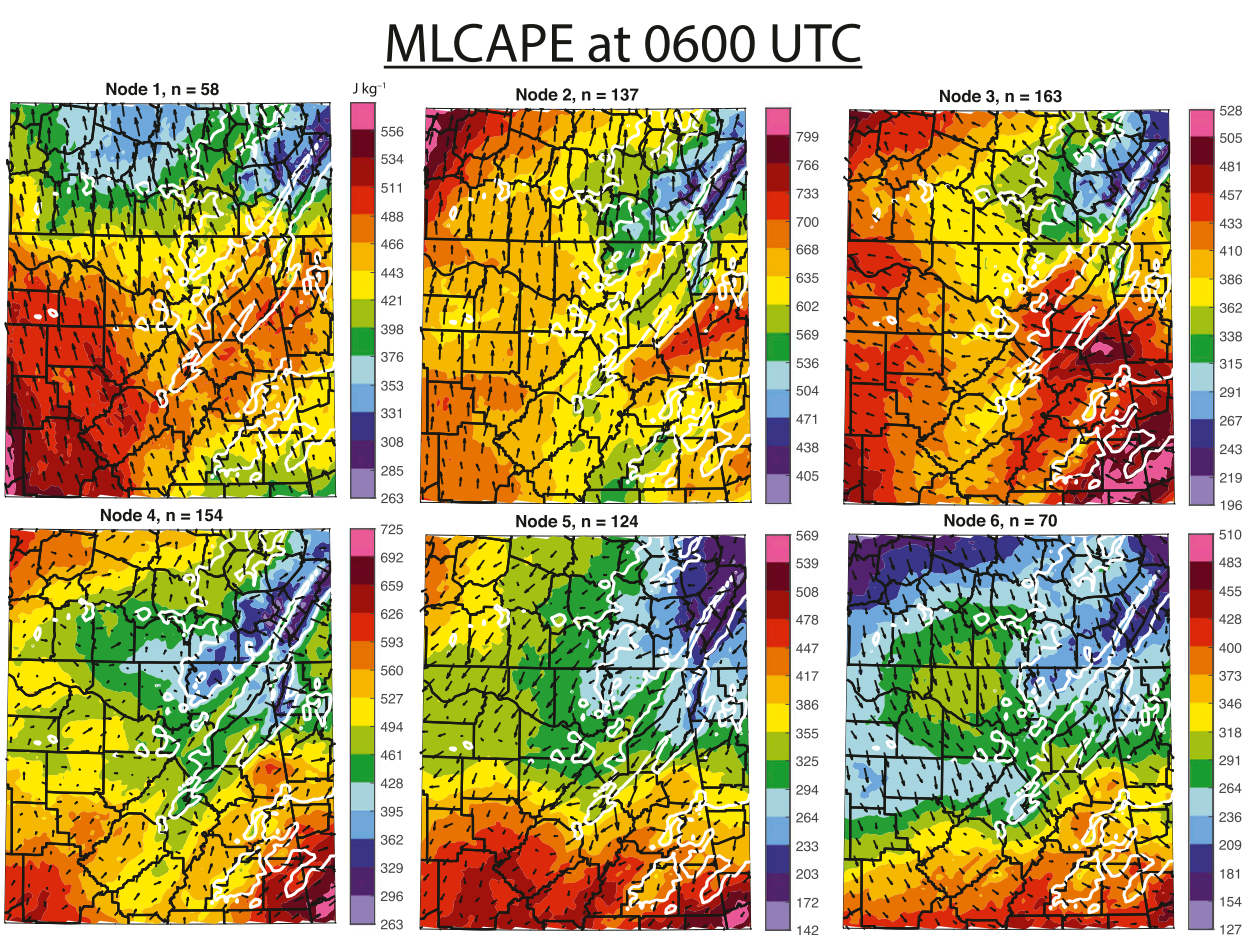

FIG. 10. As in Fig. 5, but valid at 0600 UTC.

Although perturbations to diurnal SRH01 are well correlated to local terrain contours, SRH01 at night exhibits much less correlation to terrain features. SRH01 in each of the nocturnal nodes is greater than in the diurnal nodes (Fig. 12), which is expected, particularly during tornado events (Anderson-Frey et al. 2016). In node 1, there is some indication that SRH01 is locally maximized on the western edge of Sand Mountain with slightly reduced values extending into the Tennessee Valley (Fig. 12). However, the maximum values on top of Sand Mountain ($\sim$180 $m^2 s^{-2}$) are comparable to other local maxima found across much of northern Alabama not near significant relief. In the remaining nodes, it is more difficult to identify perturbations that appear well correlated with terrain. It is possible that during strongly forced severe weather events where winds respond to strong surface pressure gradients, the perturbations may resemble those more in the diurnal SRH01 nodes when surface winds are strong and boundary layers are not characterized by strong static stability.

Mean nocturnal STP exhibits similar patterns in regions of complex topography as it does during the day. A slight maximum of STP exists on the western edge of Sand Mountain in node 1, which has a mean STP about 0.05–0.1 larger than in the Tennessee Valley (Fig. 13). The Tennessee Valley experiences a local STP minimum both during the day and at night in node 1. It is possible that downslope flow off the terrain (associated with a lee wave, which will be discussed in the following section) modifies the local environments that makes locations lee of the terrain less conducive to tornadogenesis. In the remaining nodes, STP is weak and does not vary much in complex terrain.

The mean convective environments highlight that terrain exerts a substantial influence on the local environment under some low-level flow regimes. On days where tornadoes most frequently occur, the environments atop the Sand Mountain and the Cumberland Plateaus appear to be more supportive of tornadoes than the surrounding low-lying areas. It appears that downslope flow off of Sand Mountain leads to increased LCL heights and a decrease in SRH01 within the Tennessee Valley which make the valley locally unfavorable for tornadoes when compared with observations of tornadic environments. On the other hand, SRH01 can be locally maximized in the Tennessee Valley as opposed to on top of the higher terrain when the prevailing wind direction is oriented west of the valley's orientation such that the wind within the valley becomes backed relative to the prevailing flow (e.g., Fig. 7, node 2). Most importantly, the impacts of these environmental perturbations on real storms are unknown. The influence of environmental heterogeneity on storms is poorly understood, and it is not

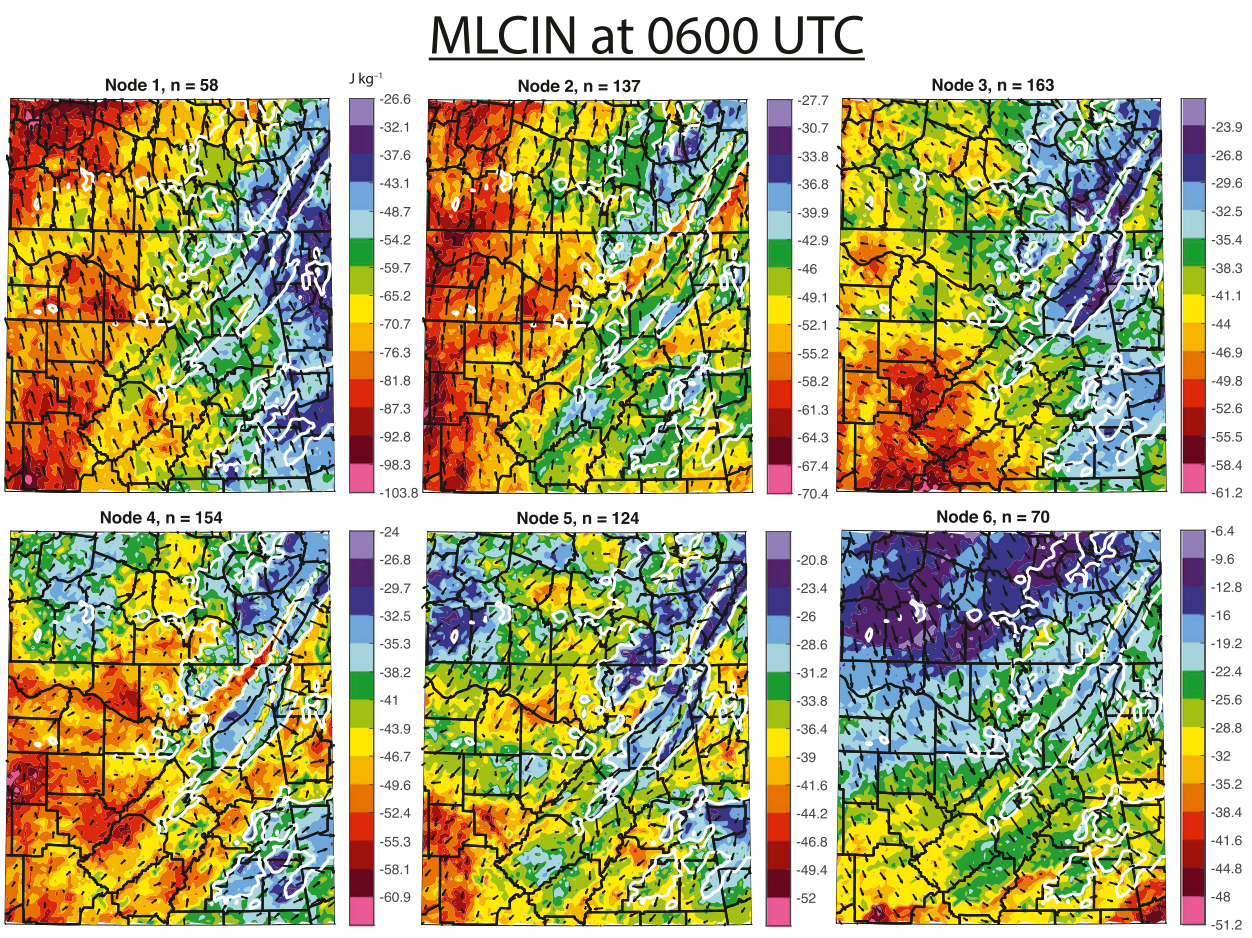

FIG. 11. As in Fig. 6, but valid at 0600 UTC.

clear how storms realize environmental changes induced by terrain. It seems unlikely that as soon as storms encounter a more favorable environment, they are immediately more prone to undergoing tornadogenesis. The terrain-induced perturbations described here are by no means the only ways that terrain is able to modify the flow and local convective environments, but are the ways that seem to be most prevalent within the climatologies focused on northeastern Alabama.

3. Simulations of convective environments in complex terrain

a. Methods

The climatologies of convective environments in the SOM analysis show many perturbations to the parameters in regions of complex topography. While it is possible to infer their origins, an idealized model approach is used here to describe how terrain may induce these perturbations. The HRRR climatologies (particularly node 1) show similarities to recent observations of SRH and LCL height near Sand Mountain (Lyza and Knupp 2018; Lyza et al. 2020). The HRRR appears capable of predicting some of the terrain-induced modifications to CAPE, CIN, SRH, and STP. However, it is not necessarily clear *how* the Sand Mountain Plateau modifies convective storm environments in its vicinity. Lyza and Knupp (2018) observed that the modification is most likely to occur when the low-level flow contains a cross-plateau component. We use an idealized model setup to determine if a similar flow response to the terrain can be created to test this idea using environments similar to those associated with severe weather events in northeastern Alabama. Additionally, the simulations will be compared to the climatologies presented in the prior sections to clarify how the influences of terrain on the flow affect nearby convective environments.

Cloud Model 1 (CM1; Bryan and Fritsch 2002) is used to investigate the influence of realistic topography on convective environments. This model has been used to simulate flow in regions of complex topography using environments characteristic of severe convective storms (e.g., Soderholm et al. 2014) and is well suited for this purpose. Our approach here is to initialize the model with a homogeneous environment until it reaches a pseudosteady state. We examine how terrain modifies the flow and how terrain-induced heterogeneity compares to the HRRR climatologies.

The model runs are simple and neglect processes represented in the HRRR from which the climatologies are derived.

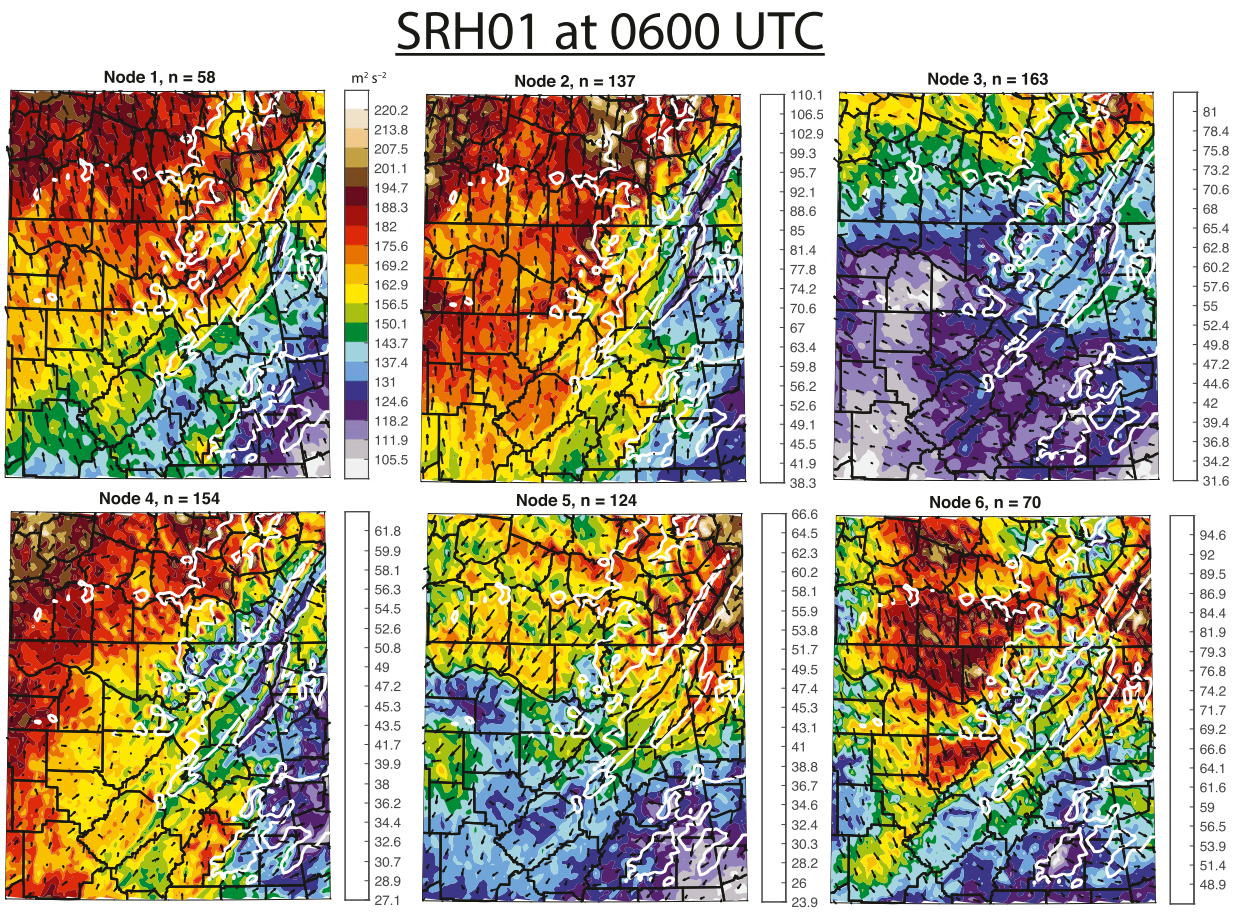

FIG. 12. As in Fig. 7, but valid at 0600 UTC.

The model domain is 400 km × 400 km × 20 km. The horizontal grid spacing is 1 km. Vertical grid spacing is 100 m below 3 km, stretches from 100 to 500 m between 3 and 12 km, and remains 500 m above 12 km. A Rayleigh damping layer is implemented above 15 km in order to limit the reflection of gravity waves from the model top toward the surface. The upper and lower boundaries are free slip, and the lateral boundaries are open radiative. The model is integrated using a third-order Runge–Kutta scheme and a fifth-order weighted essentially nonoscillatory (WENO) advection scheme (Jiang and Shu 1996). The time-splitting method of Klemp and Wilhelmson (1978) is used with a long time step of 5 s and a short time step of 0.4 s. A 1.5-order TKE scheme is used to resolve subgrid-scale turbulence (Deardorff 1980). The shape of the lower boundary is derived from the terrain of northeastern Alabama. Terrain heights from the U.S. Geological Survey digital elevation model are regridded to 1-km resolution for longitudes between 84° and 87°W and latitudes between 33° and 36°N. The terrain shape is kept within a 75-km radius near the center of the Sand Mountain Plateau. The terrain height linearly decays to 0 m in a 50-km radius beyond the full terrain. The terrain height is reduced by 200 m since 200 m is roughly the average height above sea level for regions surrounding Sand Mountain. Areas with negative terrain heights are brought up to 0 m. Finally, wavelengths shorter than $6\Delta x$ are filtered from the terrain to reduce the generation of poorly resolved waves (Soderholm et al. 2014). No land surface model is used, and the influences of radiation and the Coriolis force are neglected.

Neglecting fluxes of heat, moisture and momentum from the ground, solar radiation, and the Coriolis force all help ensure that the far field environment in the model remains constant over time. Fluxes of heat and moisture away from the surface can be important in the evolution of the mesoscale environment but would act to temporally evolve the environments. Solar radiation is important in the development of mountain–valley wind systems, but the role of these circulations on the evolution of convective environments near terrain is likely minimal in the presence of strong boundary layer flow typical of many severe weather events. Surface friction will act to slow the boundary layer winds over time in the absence of a large-scale pressure gradient force and the Coriolis force. Under this approach, only the airflow over and around the terrain is allowed to affect the convective environments. If the patterns seen in the CM1 simulations correspond well with those seen in the HRRR, it can be implied that terrain-modified flow is likely the reason for many of the small-scale perturbations in the climatologies seen near regions of complex terrain.

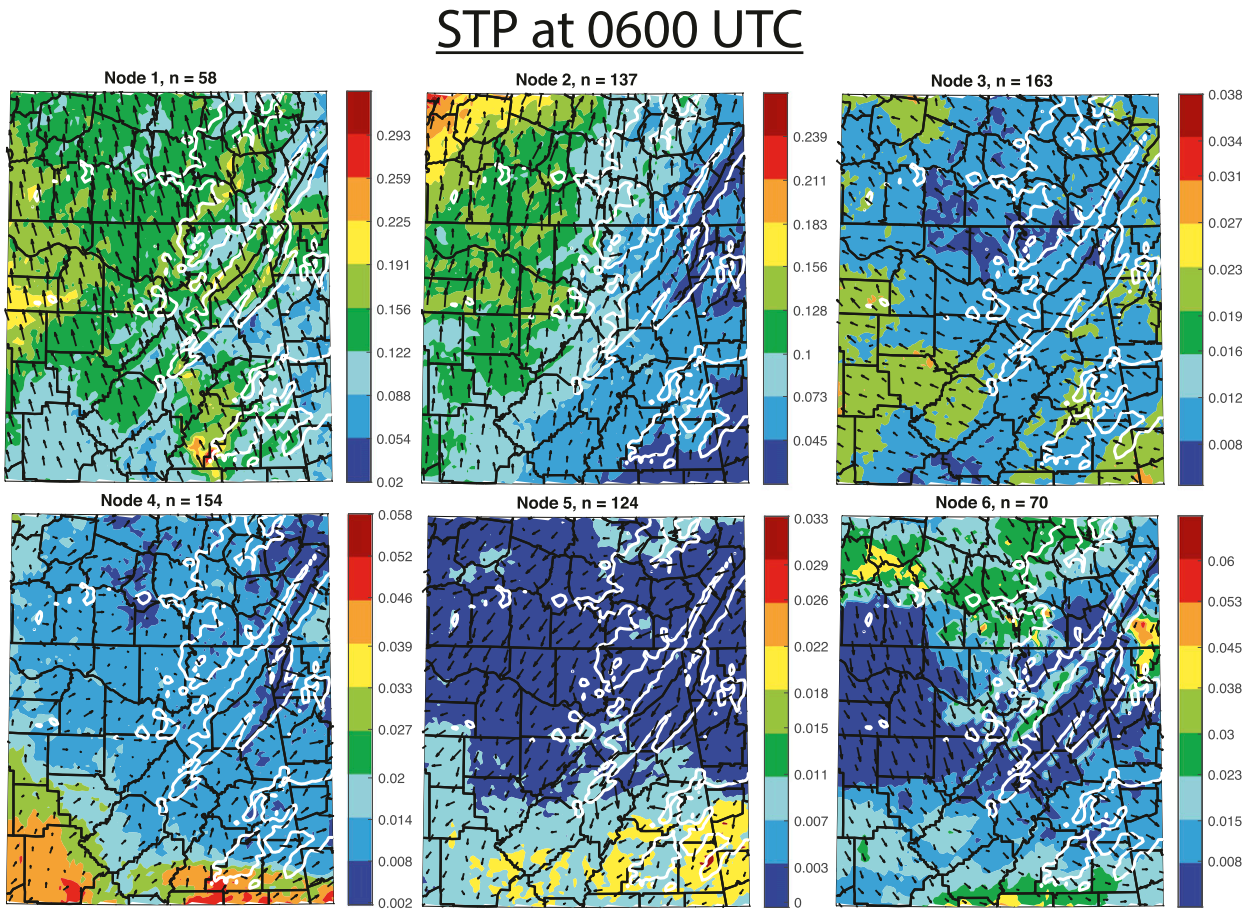

FIG. 13. As in Fig. 8, but valid at 0600 UTC.

Two different convective environments are derived from the HRRR to serve as the initial conditions for the model integration. The environments are derived from 2-h forecasts of wind speed and direction, temperature, and mixing ratio from the HRRR. The environments are taken from days on which tornadoes and other convective hazards occurred in northeastern Alabama. Additionally, the profiles were all able to be manually modified such that the Richardson number (Ri) $>$ 0.25 within the boundary layer without significantly altering the CAPE or CIN (although these necessarily changed some). The two profiles discussed below were the two that permitted long (12 h) simulations without changes to the vertical profiles of temperature, moisture, and wind over time (not due to terrain). All variables are averaged over a 9 km $\times$ 9 km square (3 grid points $\times$ 3 grid points) in order to reduce the effects of supersaturation at any one grid point. One environment contains wind directions in the boundary layer largely parallel to the plateaus in northeastern Alabama and the other environment has wind from the south, approximately 45° perpendicular to the plateaus. Environments containing wind directions perpendicular to the plateau have been observed to be more susceptible to terrain-induced modification (Lyza et al. 2020).

The parallel flow (hereafter SW flow) case was derived from a severe weather event that occurred on 5 April 2017. This case is most similar to one that would be sorted into the diurnal node 2. Temperature, pressure, water vapor mixing ratio, and wind speed and direction in a 9 km $\times$ 9 km square centered at 33.51°N 86.81°W (Birmingham, Alabama) were averaged from a 2-h HRRR forecast valid at 2100 UTC 5 April 2017. The HRRR environment (Fig. 14) contained a dry adiabatic potential temperature profile in the boundary layer. Dry adiabatic potential temperature profiles combined with strong vertical wind shear are able to exist in real severe weather environments that have forcing from the surface to maintain the boundary layer structure and large-scale pressure gradients that maintain vertical wind shear at low-levels. Mechanical mixing can reduce low-level vertical wind shear (e.g., Coffer and Parker 2015), and the effects of mechanical mixing induced by Kelvin–Helmholtz instability can be reduced by increasing static stability within the boundary layer (Fig. 14). The modified SW flow temperature profile contains an inversion near the surface reminiscent of the boundary layer structure of an early evening transition where the surface begins to radiatively cool (Fig. 14). Without this inversion, mechanical mixing drastically reduces wind shear within the lowest kilometer above the surface. Mechanical mixing does not occur during integration, as the thermal profile does not change and horizontal wind speeds vary by less than 0.2 m s^{-1} during the 12-h model integration.

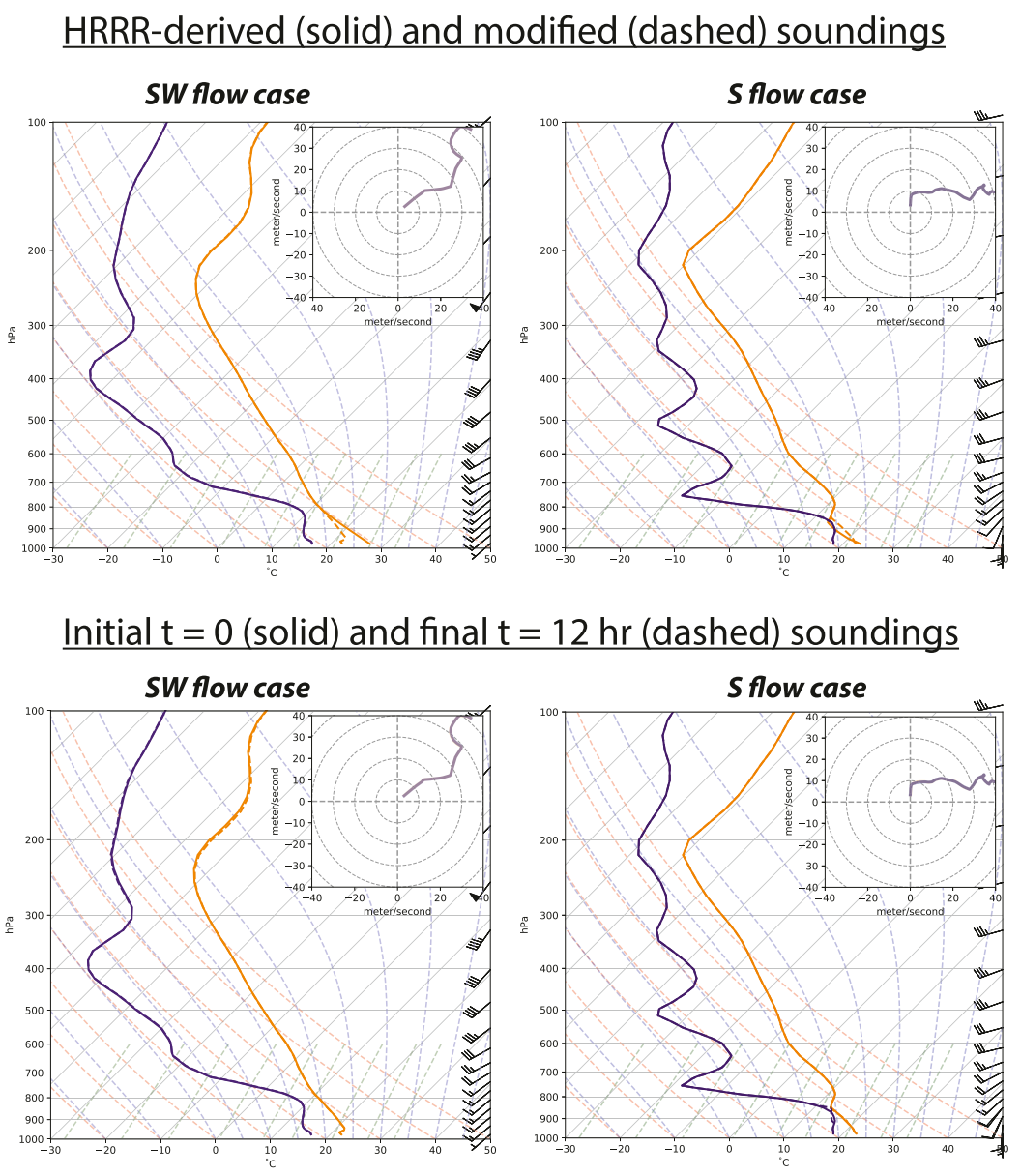

FIG. 14. (top) Soundings derived from the HRRR (solid) and modified for use in CM1 (dashed). (left) The SW flow case and (right) the S flow case. (bottom) The modified sounding at $t = 0$ (solid) and $t = 12$ h (dashed) for SW and S flow cases.

The environment containing perpendicular flow (hereafter the S flow case) is derived from a severe weather event that occurred on 19 March 2018. This case is most representative of one that would be sorted into node 1. This environment was derived from the mean conditions within a 9 km × 9 km box centered on 33.51°N, 86.81°W. Slight supersaturation was present at the top of the boundary layer, which was removed by manually warming the top of the boundary layer while cooling the surface. This slight increase in static stability (Fig. 14) was enough to remove the supersaturation, prevent moist absolutely unstable layer (Bryan and Fritsch 2000) formation, and prevent mechanical mixing from removing vertical wind shear within the boundary layer. The initial and final model states using the modified soundings are virtually identical (thermal profiles are nearly identical and horizontal wind speeds again change by less than 0.2 m s^{-1}), resulting in pseudosteady flow over the last several hours of model integration.

b. Results

The southwest flow case shows what may happen when winds are largely parallel to the terrain features in northeast Alabama. Initially, the environment contains a slight inversion near the surface and southwesterly winds that remain unidirectional for up to 1 km AGL (Fig. 14). After about 6 h, the

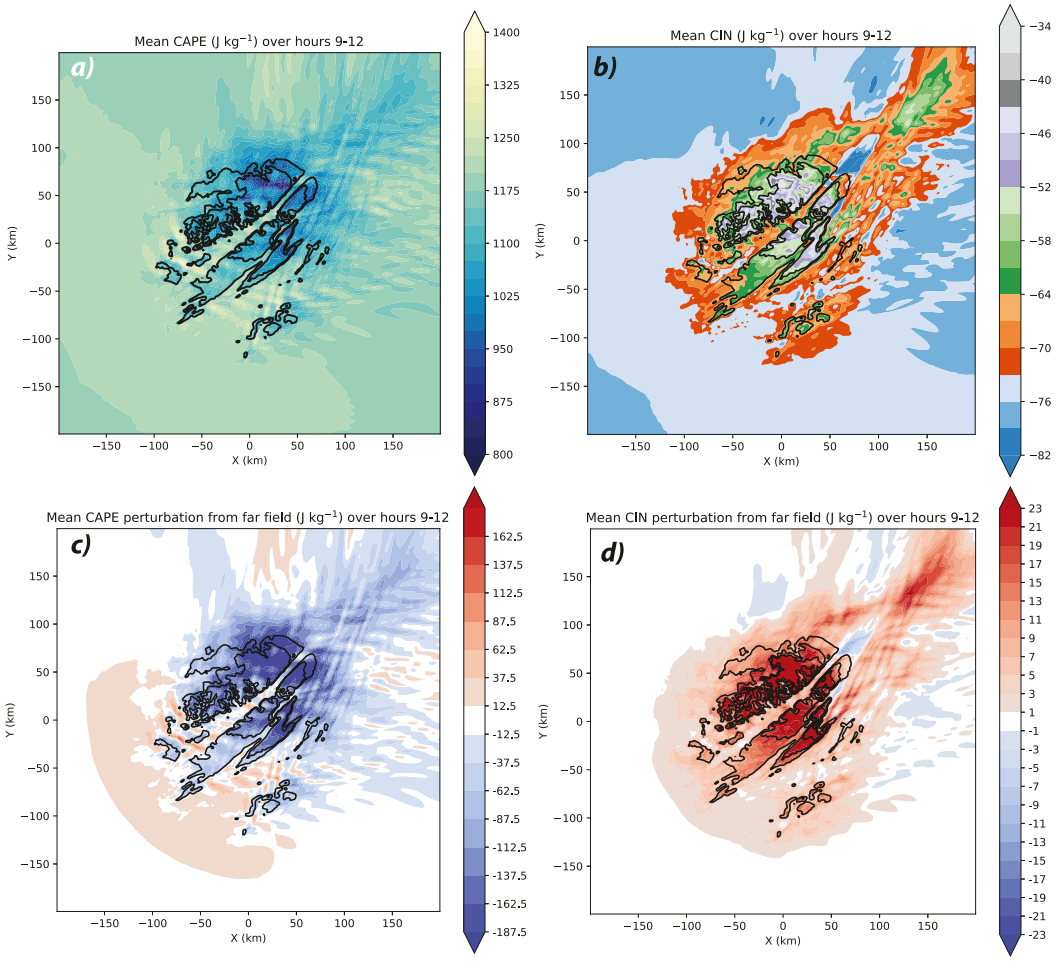

FIG. 15. (a) Mean CAPE over hours 9–12 in the SW flow simulation. Black contours show terrain heights at 100 and 200 m. (b) Mean CAPE perturbation from the value at the point located in the SW corner of the domain (−200 km, −200 km) over hours 9–12. (c) As in for (a), but for CIN. (d) As in (b), but for CIN.

flow field is fairly steady and output at 15-min intervals looks very similar to the fields created by averaging 15-min output over hours 9–12 of integration.

There is some variation in CAPE and CIN over most of the terrain system, as most elevations above 100 m experience a reduction in CAPE of about 10%–15% from the far field values (Fig. 15b). MLCAPE in node 2 is slightly increased on top of the Sand Mountain Plateau (Fig. 5), which is opposite of what is seen in the simulation. A 10%–15% change in CAPE is likely not uncommon over short distances. Since the vertical profiles of potential temperature and moisture in the far field and over the plateau show few differences (Fig. 16), it is possible these changes are attributable to the sounding modification. CIN is less negative over the higher terrain by 10–20 J kg^{-1}, an decrease in magnitude of about 25% from the far field values (Figs. 15c,d). This decrease in CIN is likely due to potential temperature being warmer atop the plateau with dewpoint temperatures being very similar to far field values (as described in section 3). CIN magnitude is also reduced on top of the higher terrain within the node 2 climatology (Fig. 6). Regions of locally higher topography are usually preferred locations for convective initiation on some days and may be regions where convection temporarily strengthens as it encounters less CIN.

SRH01, LCL heights, and STP are all relatively unperturbed near complex terrain under southwesterly flow. SRH01[1] varies by ±25 m^2 s^{-2} in the gravity waves produced by the flow over terrain in a stable boundary layer (Figs. 17a,b). These changes are well within the range of spatial SRH variability that have been observed in the boundary layer (Markowski et al. 1998; Markowski and Richardson 2007). Decreases in SRH01 are seen over terrain higher than 200 m (Figs. 17, 16). The climatology for node 2 shows a slight backing of the winds within the valley that, in the mean, lead to an increase in SRH01 locally. However, in this simulation, the winds are almost perfectly aligned with the valley, and SRH01 changes little within the

[1] The 0–1-km SRH here is calculated between the lowest vertical model grid level (50 m) and 1050 m. The storm motion used is calculated using the empirical method from Bunkers et al. (2000).

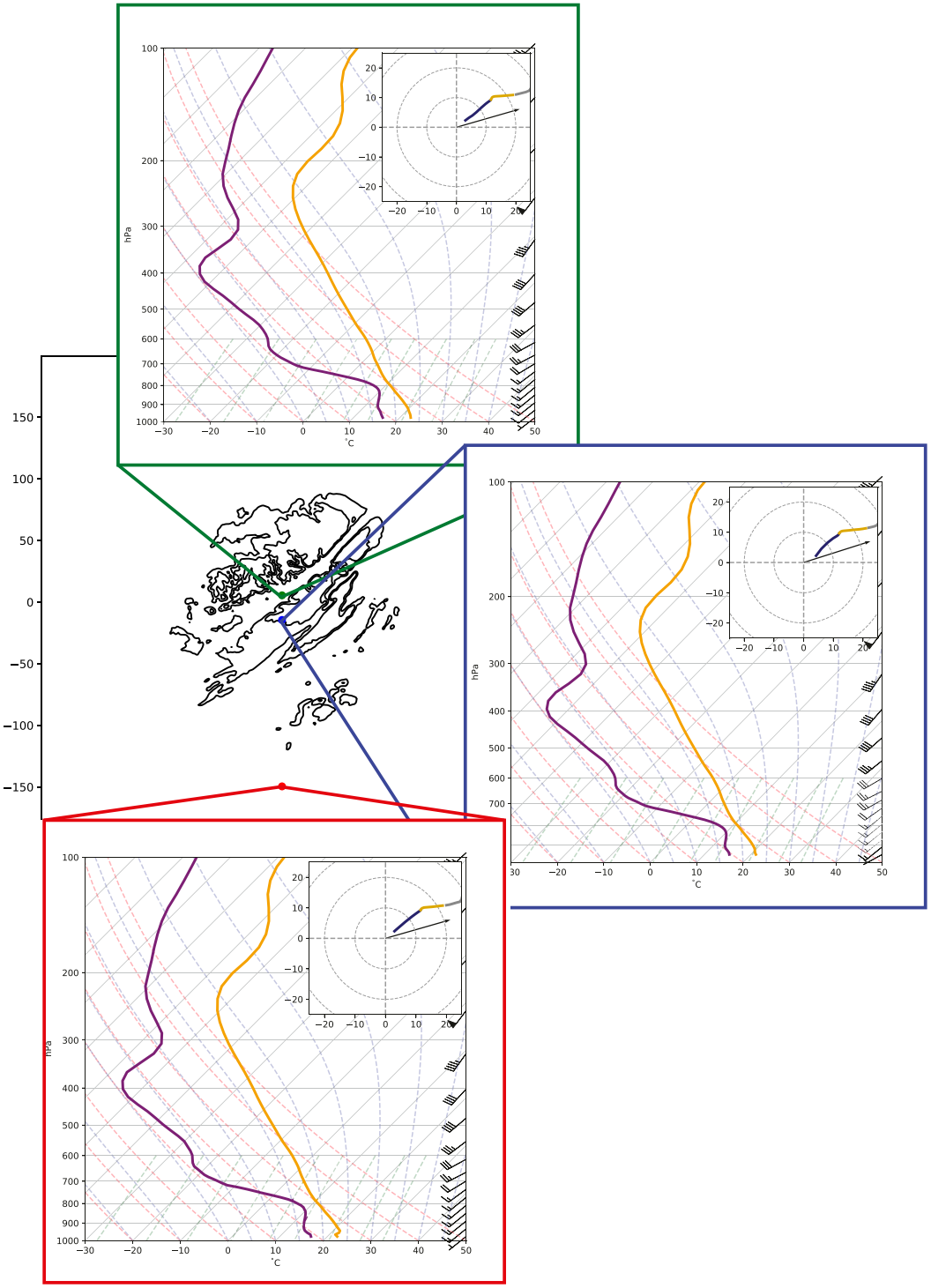

FIG. 16. The plot with black contours shows and colored dots shows constant elevation contours at both 100 and 200 m. Mean soundings over hours 9–12 at three points within the domain: the far field (red), the Sand Mountain Plateau (blue), and the Tennessee Valley (green). The orange line on the skew T–log$P$ diagram is the temperature (°C), and the purple line represents the dewpoint temperature (°C). Wind barbs show the mean wind (m s^{-1}) at every fourth vertical grid level. The inset hodograph shows the mean winds over hours 9–12 at each point. The blue segment shows the mean winds from 0 to 1 km, and the gold segment shows the mean winds (m s^{-1}) from 1 to 3 km. The gray portion of the hodograph is the mean wind winds at model levels between 3 and 6 km. The black arrow in each hodograph shows the mean storm motion at each point calculated using the Bunkers et al. (2000) approximation.

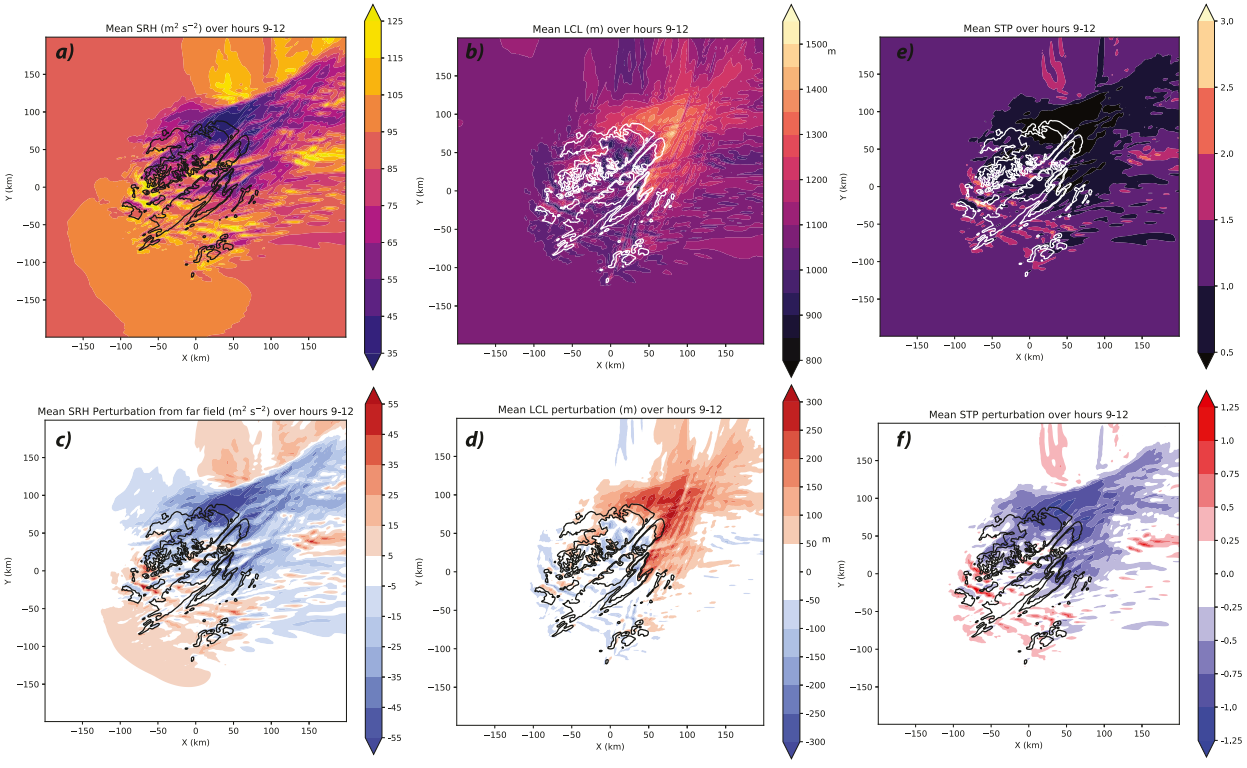

FIG. 17. (a) Mean SRH01 for in the SW flow case over hours 9–12. (b) Mean SRH perturbation from the far field over hours 9–12. (c) As in (a), but for LCL height. (d) As in (b), but for LCL height. (e) As in (a), but for STP. (f) As in (b), but for STP.

valley. LCL height relative to far field values varies by less than 50 m atop the plateaus (Fig. 17d). This is generally not consistent with the patterns seen in the SOM climatologies. There is little meaningful change in STP in the complex terrain (Figs. 17e,f). The changes in CAPE, LCL height, and SRH01 atop the plateau are relatively small compared to the background values, and the result is little change in STP. STP shows little variation near complex terrain in node 2 (Fig. 8). Without a strong cross-terrain component, the convective environments remained relatively unchanged around the complex terrain.

The southerly flow regime impinging on the plateau at roughly a 45° angle induces greater changes to convective environments near the terrain system in northeastern Alabama. Small reductions in CAPE are seen atop both plateaus and in the valley on the lee side of the Sand Mountain Plateau (Figs. 18a,b). The reduction of CAPE in the valley is associated with slightly decreased water vapor mixing ratios in the boundary layer and an associated reduction in equivalent potential temperature for near-surface parcels (Fig. 19). This small reduction in CAPE is very similar to mean diurnal MLCAPE field portrayed in node 1 (Fig. 5). CIN magnitude is decreased in the regions of higher terrain. The contours of positive changes in CIN are aligned with local terrain contours (Fig. 18d). CIN is weaker atop the regions of higher terrain because the surface-based parcels are characterized by higher equivalent potential temperatures (Fig. 19). Weak CIN is also found on top of the plateaus in node 1 (Fig. 6). The distributions of CAPE and CIN around the plateau and valley system closely resemble those in the node 1 mean fields.

SRH01 is sensitive to terrain-modified flow in the southerly flow case. SRH01 on top of the Sand Mountain Plateau is 5–25 $m^2 s^{-2}$ larger than far field values and decreases of a similar magnitude are seen in the Tennessee Valley (Figs. 20a,b). Such differences in SRH01 from the plateau top to the valley floor are seen in node 1 (Fig. 7). Lyza et al. (2020) documented a strong increase in SRH01 near the base of the Sand Mountain Plateau, but this increase is not seen here. This could be due to differences in upstream environments or the idealized nature of these simulations and their relatively large horizontal grid spacing. The increase in SRH01 on top of the plateau is associated with increased vertical wind shear on top of the plateau (Fig. 21b), which leads to greater streamwise vorticity in the lowest 300 km AGL atop the plateau (Fig. 21c). Since storm-relative winds are predominantly easterly atop the plateau (Fig. 19), an increase in magnitude of the negative x component of vorticity would increase the streamwise vorticity just above the surface. The stronger vertical wind shear atop the plateau is likely a consequence of parcels originating at levels below the plateau top decelerating as they work against environmental static stability to ascend the plateau. Parcels near and higher than 250 m above sea level do not experience as much vertical displacement and subsequent deceleration. As a consequence, vertical wind shear is stronger atop the plateau because of the reduced vertical distance between weaker near-surface wind and stronger wind aloft, implying stronger horizontal vorticity that is aligned with the easterly storm-relative winds near the surface. A similar increase in vertical wind shear

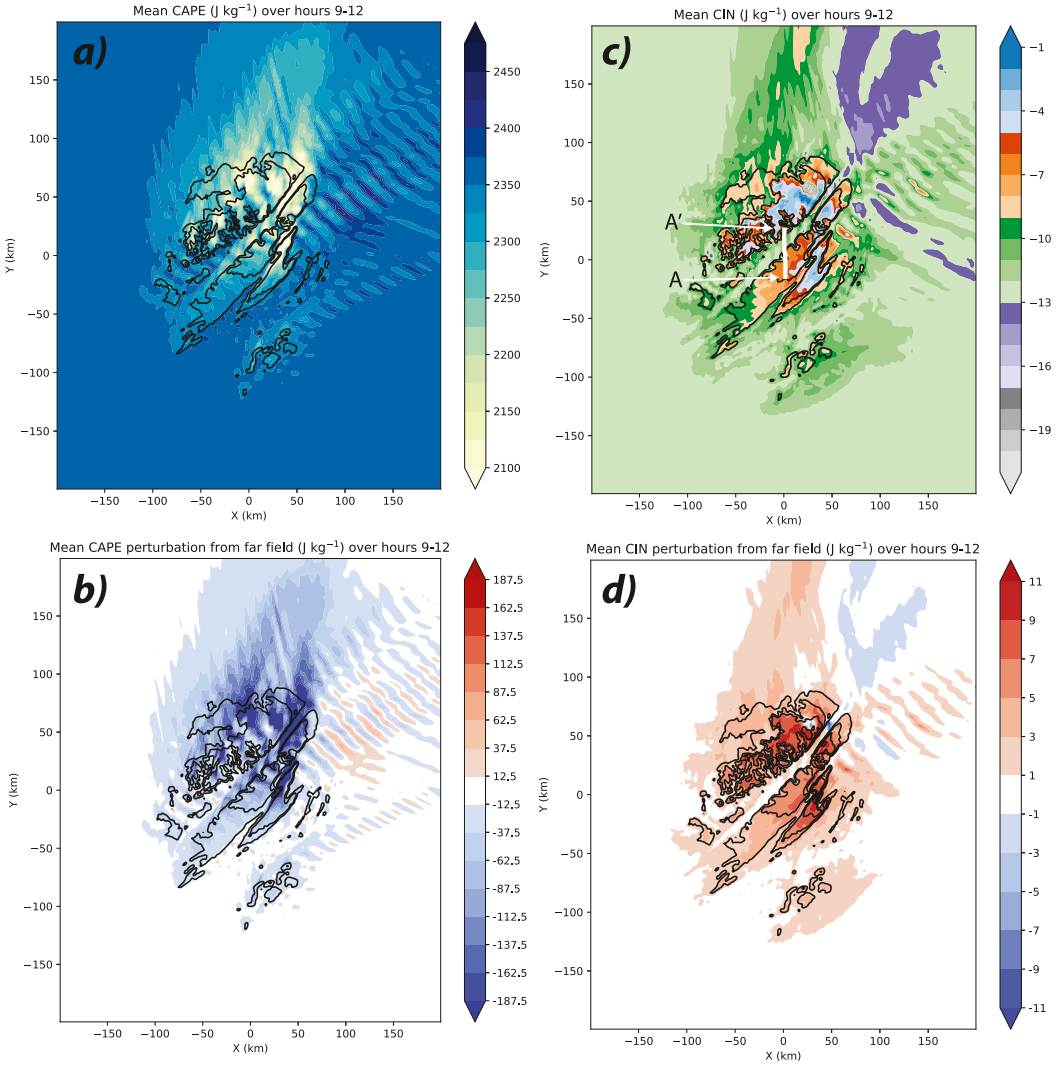

FIG. 18. (a) Mean CAPE over hours 9–12 for the S flow case. Black lines represent terrain height at 100 and 200 m. (b) Mean CAPE perturbation over hours 9–12. (c) As in (a), but for CIN. The white line shows the location of the cross sections shown in Fig. 21. (d) As in (b), but for CIN.

may exist atop the plateau without a stable boundary layer owing to surface friction. It has been hypothesized that friction acting on the parcels as they cross the broad plateau may lead to the development of a mechanical internal boundary layer atop the plateau, which would also act to increase vertical wind shear (Lyza and Knupp 2018). Because the simulations performed here included a free slip lower boundary, it was not possible to assess this mechanism as one that might act to influence SRH01 atop Sand Mountain.

The SRH01 decrease within the Tennessee Valley results from an acceleration of the near surface wind speeds in the valley (Figs. 19 and 21a). The decrease in SRH is largely due to decreased streamwise vorticity in the 300–1000 m AGL layer within the valley (Fig. 21c). Flow acceleration within the lee wave decreases low-level wind shear, particularly within this aforementioned layer. Such flow accelerations on the lee of Sand Mountain have been observed on days where the environment was supportive of convective storms (Lyza et al. 2020). This fairly uniform increase in wind speed throughout the lowest kilometer of the atmosphere reduces vertical wind shear and streamwise vorticity, which in turn reduces SRH01. The increase in wind speed is associated with a standing wave that develops in the lee of Sand Mountain (Figs. 22a,b).

The development of a lee wave in this regime is investigated in the context of observed lee waves near the Sand Mountain Plateau. The development of lee waves depends on both the height and width of the obstacle (Hunt et al. 1988; Vosper et al. 2002). The parameter $\mathrm{Fr}_H = U/(NH)$ should be >1 so that parcels can pass over the terrain, and the parameter $\mathrm{Fr}_L = U\pi/(NL)$ should be <1 for lee wave development, where U is a characteristic horizontal velocity normal to the terrain, N is the Brunt–Väisälä frequency, H is the characteristic terrain height (250 m here), and L is the characteristic length scale of the terrain (40 km). We calculate Fr_H and Fr_L as in Lyza and Knupp (2018).

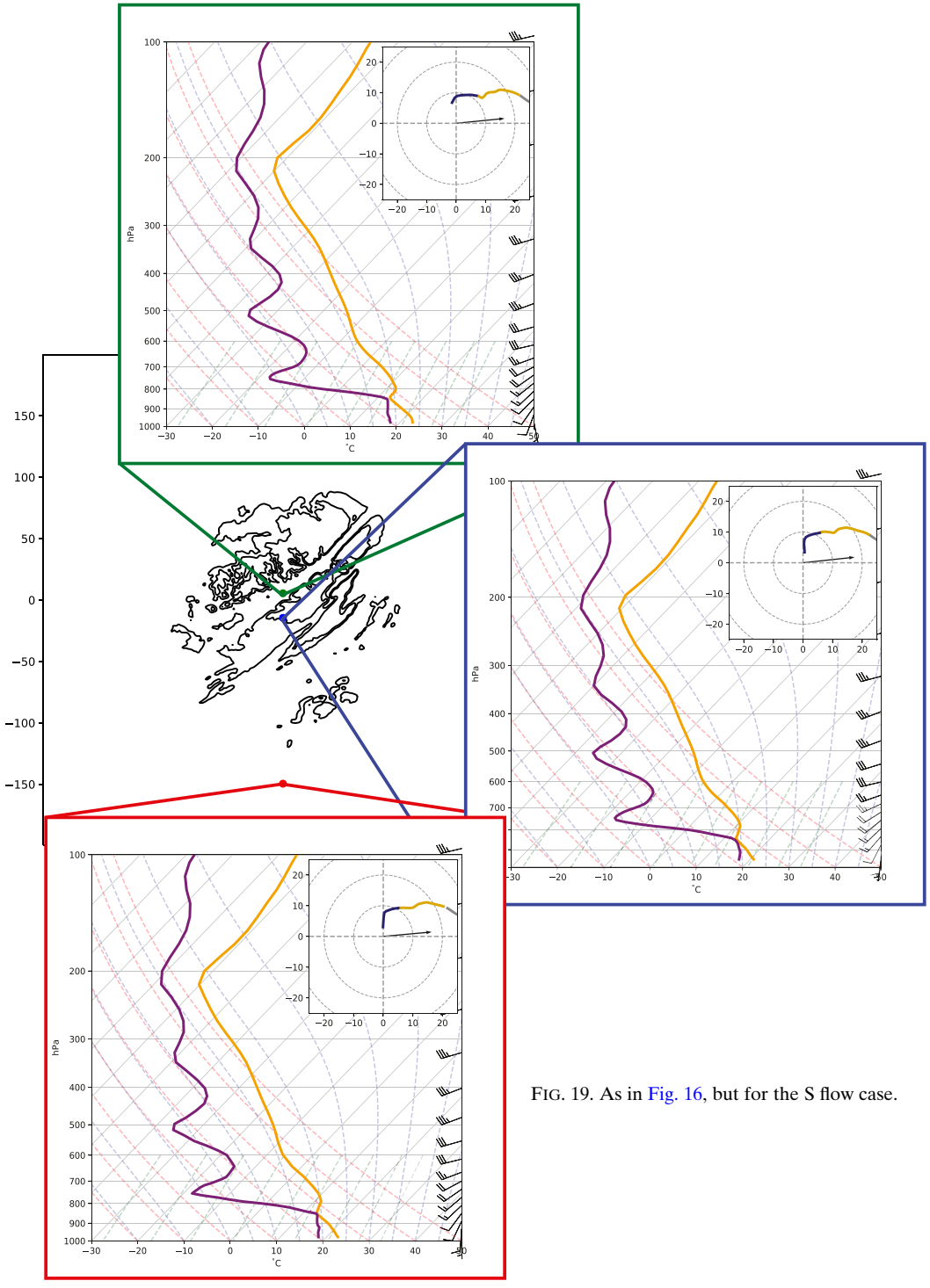

FIG. 19. As in Fig. 16, but for the S flow case.

The mountain Froude number (Fr_H) calculated for flow up stream of the 250-m-tall plateau is between 0.25 and 0.7 in the lowest 500 m, owing to the stability of the lower level and a somewhat weak orthogonal component of the wind relative to the hill's major axis. Fr_L is much less than 1 (0.005–0.015) in the lowest 500 m. Based on the Froude numbers for the initial vertical profile, lee wave development should not exist. However, the presence of this lee wave and associated downslope wind enhancement is clear in vertical cross sections (Fig. 22). This lee wave is similar to one observed by Lyza et al. (2020), which occurred for conditions that satisfied the theory of Hunt et al. (1988). We may see a lee wave on the northwest side of the

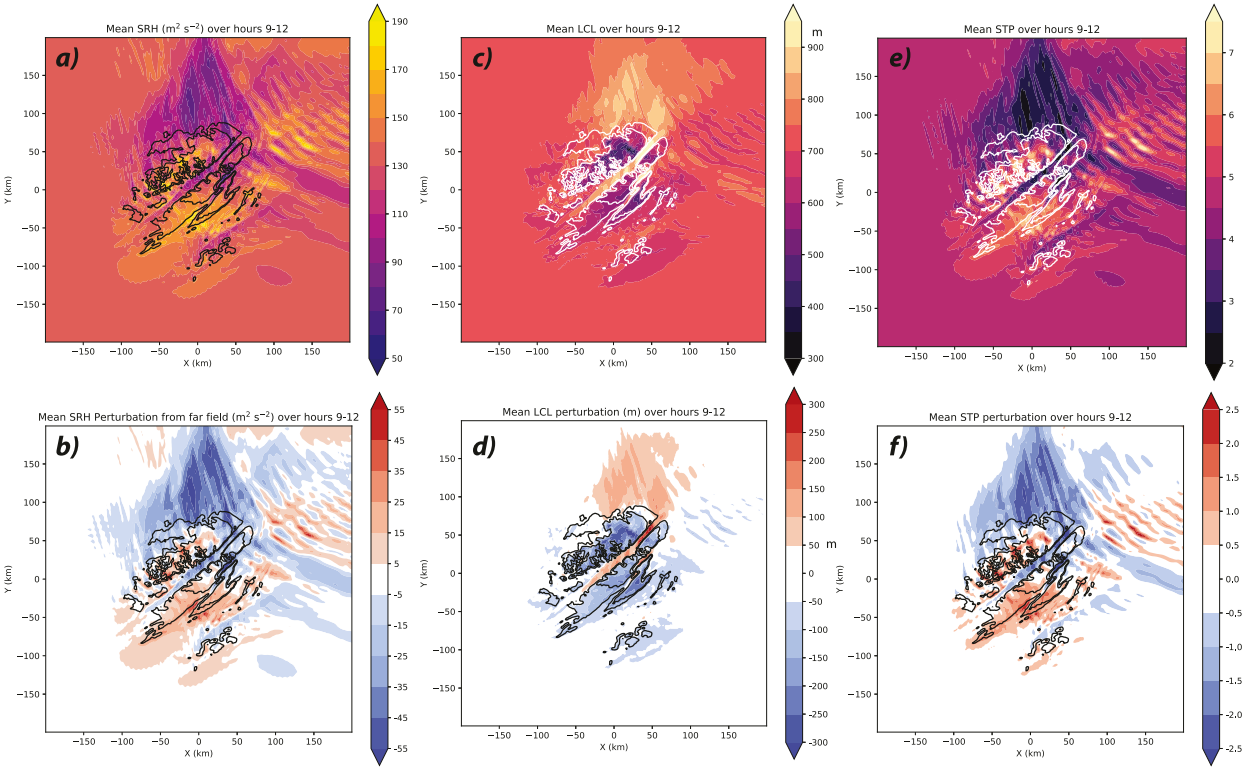

FIG. 20. Mean SRH over hours 9–12 for the S flow case. Black and white contours represent constant height contours at 100 and 200 m. (b) Mean SRH perturbation over hours 9–12 for the S flow case. (c) As in (a), but for LCL height. (d) As in (b), but for LCL height. (e) As in (a), but for STP. (f) As in (b), but for STP.

plateau in our simulations because it is not clear where Fr_H and Fr_L should be calculated in order to best characterize the flow. Perhaps the flow is only partially blocked, and the flow that ends up crossing the terrain contributes to the wave breaking. Additionally, the presence of directional wind shear may influence the generation of mountain waves (e.g., Doyle and Jiang 2006), and the influence of directional shear is not captured in the Froude number calculations.

The wave itself may be more important in modifying the low-level wind shear pattern near the terrain rather than directly modifying storms traveling through the standing wave. While there is some evidence that lee waves may affect linear convection in the vicinity of plateaus (e.g., Booker 1963), the effects of this wave on a supercell (as opposed to the environment) are uncertain. Negative vertical velocity exceeding $0.5\,m\,s^{-1}$ and negative vertical vorticity between 1 and $2 \times 10^{-3}\,s^{-1}$ exists within this wave as flow is accelerated into the valley (Fig. 22). These values are an order of magnitude or two smaller than the positive vertical velocity and vertical vorticity found in supercell storms, so they are likely negligible in terms of inhibiting tornadogenesis. This lee wave appears to be important for modification of the local convective environment in the vicinity of the plateau, but its influence on storms themselves remains unclear.

Perturbations of LCL height and STP are well correlated with terrain height contours. Negative LCL height perturbation contours are largely confined to the higher terrain and the magnitude of the perturbation is equal to the height of the terrain above sea level (Figs. 20c,d). In the valley, the 50-m increase in LCL height appears to be associated with a slightly warmer and drier boundary layer (likely resulting from downslope flow) than the far field (Fig. 19). STP varies greatly from atop the plateaus to the valley. STP in the far field is about 4.5, which indicates that the environment is capable of supporting strong tornadoes (Thompson et al. 2003). STP is reduced from far-field values by about 1 within the valley and increased by about 1 on top of the plateau. A qualitatively similar pattern of STP perturbations is seen within the node 1 climatologies, where STP on top of the plateau is larger than the STP in the valley to the west (Fig. 8). Tornado events in the Southeast occur across a wide range of STP values (Anderson-Frey et al. 2019), but the effects of spatial variability in STP on likelihood of tornadogenesis are unknown. It is unknown if the increase in STP seen on top of the Sand Mountain Plateau would be important in determining local tornado risk. Low-level flow regimes that contain substantial cross-terrain components are most likely to experience perturbations in local convective environments within this plateau and valley system.

4. Discussion and conclusions

The influence of complex terrain on convective environments in northeastern Alabama is highly dependent on wind direction and low-level static stability. The following

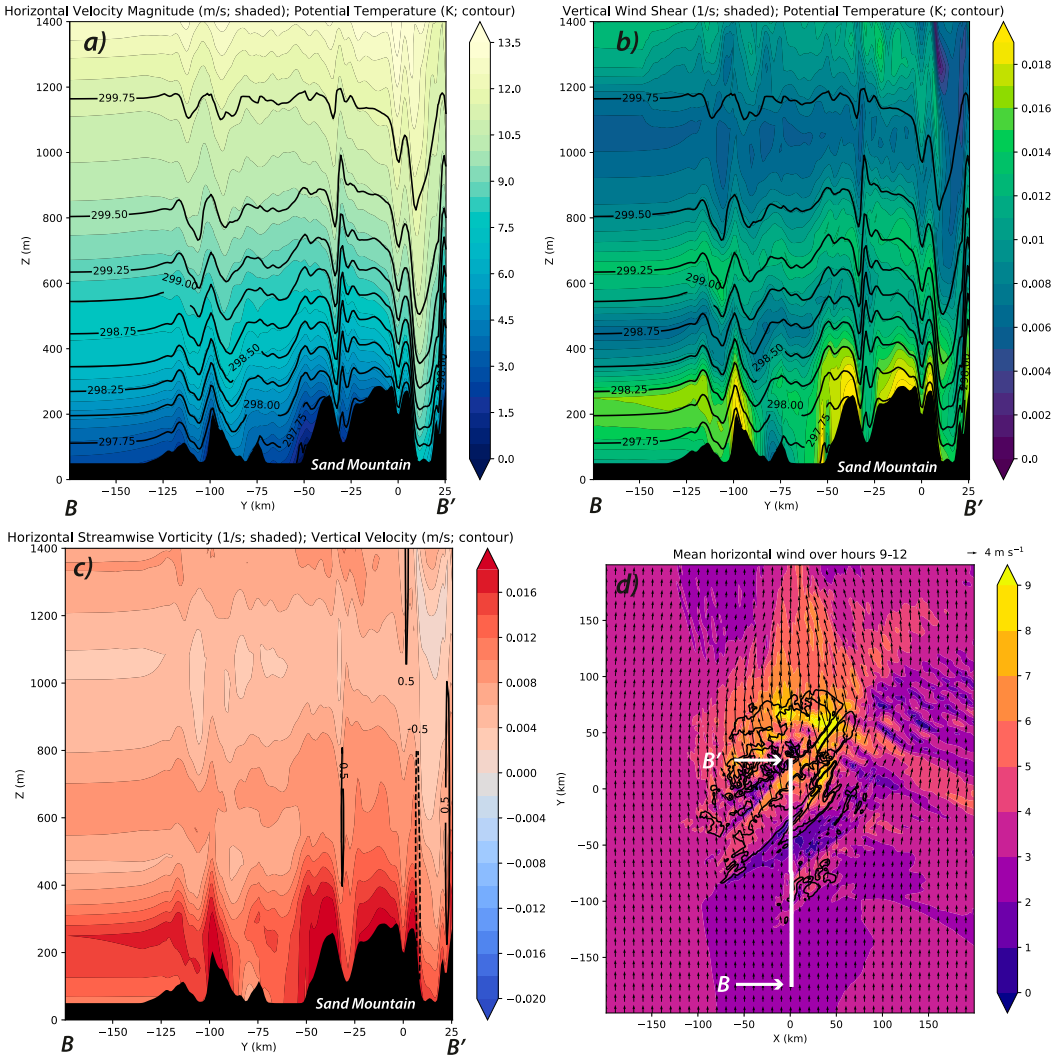

FIG. 21. (a) Vertical cross section of horizontal velocity (filled contours) and potential temperature (contours) averaged over hours 9–12. (b) As in (a), but for vertical wind shear and potential temperature. (c) As in (a) and (b), but for streamwise horizontal vorticity and contours represent vertical velocity of 0.5 m s^{-1} (solid contours) and −0.5 m s^{-1} (dashed contours) averaged over hours 9–12. (d) Mean 50 m AGL horizontal wind over hours 9–12. The black contours represent the 100- and 200-m constant height surfaces. Arrows represent the mean wind direction over hours 9–12. The solid white line represents the path of the cross section in (a)–(c).

questions posed in the introduction have been addressed through our climatology and modeling efforts and are answered below.

- *Where are terrain-induced perturbations most likely?* Terrain induced perturbations are frequently seen near the Cumberland and Sand Mountain Plateaus and within the Tennessee Valley. In the node with the most frequent occurrence of tornadoes, mean conditions on the Sand Mountain Plateau (evaluated by STP) appear to be more favorable than within the Tennessee Valley.
- *How does low-level wind direction influence where these perturbations occur?* Perturbations to MLCAPE and MLCIN are relatively insensitive to wind direction, while the locations of perturbations to SRH01 vary substantially with wind direction. Mean SRH01 is higher on top of the Sand Mountain Plateau on days with southerly flow, but on days where the flow contains a substantial westerly component, SRH01 tends to be higher in the Tennessee Valley.
- *What are the physical origins of the perturbations seen in the climatologies?* Changes in LCL height are very similar to changes in elevation, indicating that parcels on top of the plateau have to travel less vertical distance to reach their LCLs. Decreases in CIN are associated with increases in potential temperature on top of the plateau, which occurs due to the slightly stable boundary layer in the idealized simulations performed here. This is likely not be the only mechanism that leads to decreased CIN across the plateau on

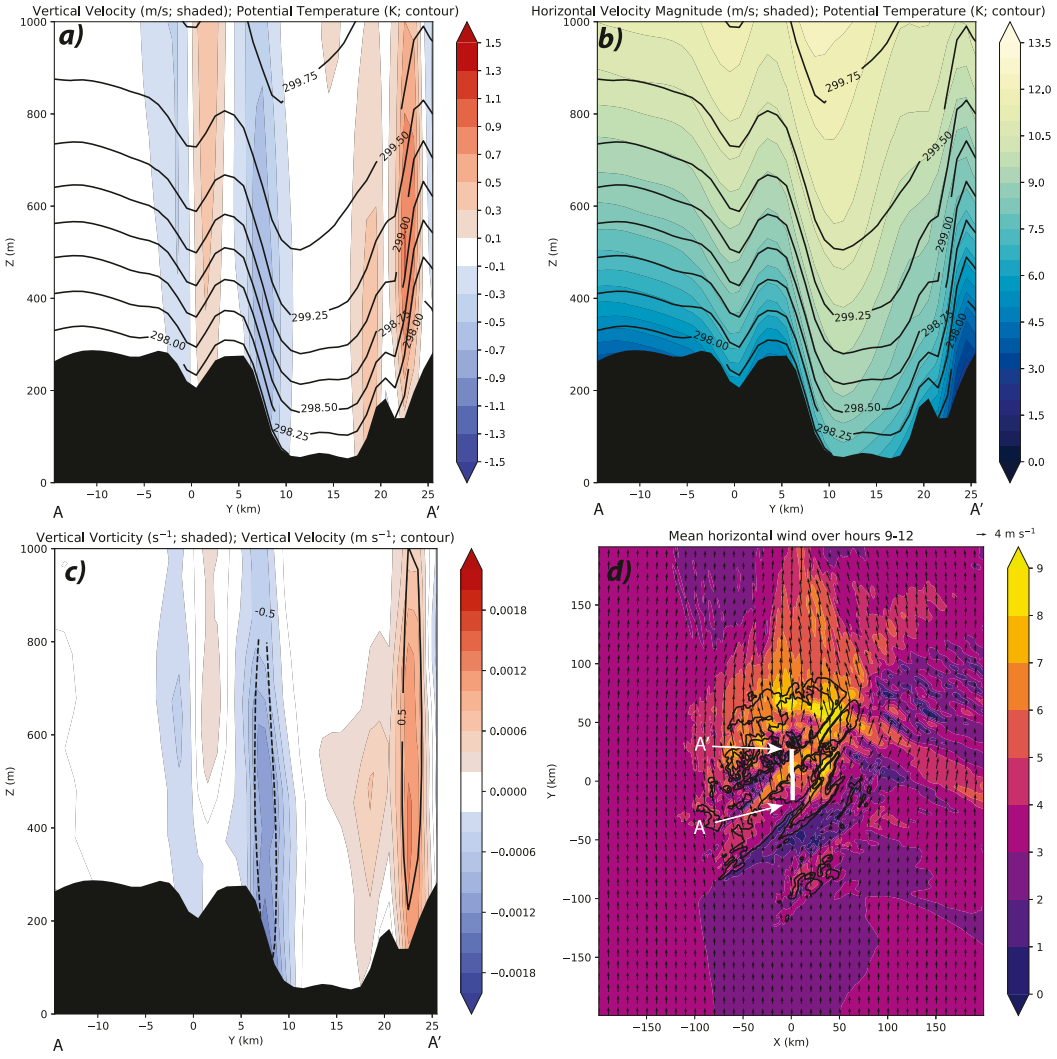

FIG. 22. (a) Vertical cross section of vertical velocity (filled contours) and potential temperature (contours) averaged over hours 9–12. (b) As in (a), but for horizontal wind speed and potential temperature. (c) As in (a) and (b), but for vertical vorticity and contours represent vertical velocity of 0.5 m s^{-1} (solid contours) and −0.5 m s^{-1} (dashed contours) averaged over hours 9–12. (d) Mean 50 m AGL horizontal wind over hours 9–12. The black contours represent the 100- and 200-m constant height surfaces. Arrows represent the mean wind direction over hours 9–12. The solid white line represents the path of the cross section in (a)–(c).

all days, particularly when the boundary layer is well mixed. CAPE is slightly smaller on the plateau in each flow case. Slight decreases in water vapor mixing ratio atop the terrain are likely the reason for these small decreases in CAPE, despite increases in potential temperature. Changes in low-level flow direction and speed are primarily associated with changes in SRH01. Backing of low-level flow relative to the prevailing flow is associated with SRH01 enhancements in the Tennessee Valley. Flow accelerations associated with a standing wave on the northwest side of Sand Mountain under southerly flow can act to locally reduce SRH01 in the valley. Additionally, increases in SRH01 are found on top of the plateau in southerly flow, resulting from enhanced vertical wind shear and streamwise vorticity.

The results presented here are similar to observations from the VORTEX-Southeast field campaign. Standing waves are likely an important mechanism for modifying low-level wind profiles near Sand Mountain and within the Tennessee Valley. Such a wave is demonstrated both within the idealized simulations presented here and by Lyza and Knupp (2018) and Lyza et al. (2020). The development of the wave is likely dependent on both low-level static stability and the orientation of the wind relative to the terrain (as characterized by the mountain Froude number). Additionally, the HRRR climatologies shown here and recent observations both show that on days when SRH01 is large, SRH01 tends to be larger atop Sand Mountain and lower in the Tennessee Valley. Direct observations (Lyza and Knupp 2018; Lyza et al. 2020), climatologies, and idealized

modeling efforts are all pointing toward the idea that as convective environments become more favorable for tornadoes in in the vicinity of Sand Mountain, the near-storm environment becomes enhanced atop the Sand Mountain Plateau. While it is still unknown how or if storms realize these terrain-induced changes in environment, the topic is certainly worth addressing in the near future.

Complex terrain is likely an important source of environmental heterogeneity on days with convective storms. However, the influence of such heterogeneity on storms remains poorly understood. Heterogeneous environments have been linked to different fates of two storms evolving in close proximity (Klees et al. 2016), where SRH01 and STP were observed to be larger in the vicinity of the tornadic storm. Spatial (Richardson et al. 2016) and temporal (Letkewicz et al. 2013; Davenport and Parker 2015; Coffer and Parker 2015; Davenport et al. 2019) heterogeneity have been shown to be important in the evolution of convective storms. However, questions remain as to how heterogeneity ultimately influences a storm's strength and how it affects tornadogenesis. Little is known about the magnitude of changes to low-level wind shear or CAPE to sufficiently affect storm strength and if these changes are relative to the initial values. Additionally, questions remain about the length of time necessary for storms to exhibit changes in mesocyclone, updraft, or near-surface circulation and how long storms must reside in these changed environments for noticeable change to occur. These unknowns affect how forecasters may be able to anticipate changes in storm morphology relative to anticipated changes in the local environment.

At this point, enough evidence exists to support the idea that terrain affects storm strength and evolution, but correlating changes in the chances for a storm to produce severe convective hazards to these terrain-induced changes cannot yet be done. To best anticipate changes in storm strength relative to terrain, storms likely need to reside in the perturbed conditions for a sufficiently long period such that the storm can change intensity. *If storm motion allows for the storm to reside in a perturbed environment for a long period of time, then one could assume that the storm would have an increased likelihood of strengthening or weakening depending on the sign of the perturbation.*

Future work should consider how storms respond to these environmental perturbations. It is virtually impossible to know what the influence of terrain is on any given storms. Over time, if enough high-quality observations can be generated, then a trend may emerge between observed changes in storm characteristics and differences in the prestorm environments in regions of complex terrain. Computer simulations are currently the best bet to determine what the influence of terrain is on convective storm hazards. Modeling allows for storms to be simulated both with and without terrain (e.g., Markowski and Dotzek 2011) and with terrain at different resolutions (e.g., Homar et al. 2003) to determine what the influence of terrain is on storm dynamics. Future research should also investigate if terrain should be a consideration in the forecasting process. If other atmospheric processes and sources of environmental variability outweigh the influence of terrain, then research efforts would be better spent understanding, observing, and forecasting the most important sources of variability in storm environments.

Acknowledgments. This work was supported by the NOAA Award NA17OAR4590189 made to The Pennsylvania State University. Computational resources were provided by the Penn State Institute for Computational and Data Sciences. We would like to acknowledge the help of Curtis Alexander, Stanley Benjamin, Art Person, and Brice Coffer in the development of the HRRR dataset used for this work. We thank George Bryan for his generous support of CM1 and for suggestions on simulating convective environments for long periods of time. We would also like to thank Alexandra Anderson-Frey for discussions on SOMs and how they might be helpful for this work. We appreciate the critical and constructive evaluations of this work by Anthony Lyza and two anonymous reviewers.

Data availability statement. HRRR data that comprise this project are openly available through multiple sources. The data used in Katona et al. (2016) comprising the years 2013–15 may be found in the Penn State DataCommons (https://www.datacommons.psu.edu/commonswizard/MetadataDisplay.aspx?Dataset=6165). The remaining years (2016–18) can be found in the Amazon Web Services repository of HRRR data (https://registry.opendata.aws/noaa-hrrr-pds/). Parts of the dataset used in Katona et al. (2016) are not available on the AWS repository, which begins in 2014. A compiled version of CM1, along with namelist files, initialization soundings, and terrain files are hosted on Katona's GitHub page (https://github.com/btkatona/VORTEX-SE-Publication). These files will allow anyone to recreate the dataset used in the idealized model runs.

REFERENCES

Anderson-Frey, A. K., Y. P. Richardson, A. R. Dean, R. L. Thompson, and B. T. Smith, 2016: Investigation of near-storm environments for tornado warnings and events. *Wea. Forecasting*, **31**, 1771–1790, https://doi.org/10.1175/WAF-D-16-0046.1.

——, ——, ——, ——, and ——, 2017: Self-organizing maps for the investigation of tornadic near-storm environments. *Wea. Forecasting*, **32**, 1467–1475, https://doi.org/10.1175/WAF-D-17-0034.1.

——, ——, ——, ——, and ——, 2019: Characteristics of tornado events and warnings in the southeastern United States. *Wea. Forecasting*, **34**, 1017–1034, https://doi.org/10.1175/WAF-D-18-0211.1.

Banta, R. M., 1990: The role of mountains in making clouds. *Atmospheric Processes over Complex Terrain*, *Meteor. Monogr.*, No. 47, Amer. Meteor. Soc., 229–283.

Benjamin, S., and Coauthors, 2016: A North American hourly assimilation and model forecast cycle: The Rapid Refresh. *Mon. Wea. Rev.*, **144**, 1669–1694, https://doi.org/10.1175/MWR-D-15-0242.1.

Booker, D. R., 1963: Modification of convective storms by lee waves. *Severe Local Storms*, *Meteor. Monogr.*, No. 27, Amer. Meteor. Soc., 129–140.

Bosart, L. F., A. Seimon, K. D. LaPenta, and M. J. Dickinson, 2006: Supercell tornadogenesis over complex terrain: The Great Barrington, Massachusetts, tornado on 29 May 1995. *Wea. Forecasting*, **21**, 897–922, https://doi.org/10.1175/WAF957.1.

Bryan, G. H., and J. M. Fritsch, 2000: Moist absolute instability: The sixth static stability state. *Bull. Amer. Meteor. Soc.*, **81**, 1207–1230, https://doi.org/10.1175/1520-0477(2000)081<1287:MAITSS>2.3.CO;2.

——, and ——, 2002: A benchmark simulation for moist nonhydrostatic numerical models. *Mon. Wea. Rev.*, **130**, 2917–2928, https://doi.org/10.1175/1520-0493(2002)130<2917:ABSFMN>2.0.CO;2.

——, G. Romine, S. B. Trier, and D. Ahijevych, 2018: Impact of terrain on supercells according to idealized simulations with actual terrain. *29th Conf. on Severe Local Storms*, Stowe, VT, Amer. Meteor. Soc., 108, https://ams.confex.com/ams/29SLS/webprogram/Paper348681.html.

Bunkers, M. J., B. A. Klimowski, J. W. Zeitler, R. L. Thompson, and M. L. Weisman, 2000: Predicting supercell motion using a new hodograph technique. *Wea. Forecasting*, **15**, 61–79, https://doi.org/10.1175/1520-0434(2000)015<0061:PSMUAN>2.0.CO;2.

Coffer, B. E., and M. D. Parker, 2015: Impacts of increasing low-level shear on supercells during the early evening transition. *Mon. Wea. Rev.*, **143**, 1945–1969, https://doi.org/10.1175/MWR-D-14-00328.1.

——, and ——, 2017: Simulated supercells in nontornadic and tornadic VORTEX2 environments. *Mon. Wea. Rev.*, **145**, 149–180, https://doi.org/10.1175/MWR-D-16-0226.1.

Davenport, C. E., and M. D. Parker, 2015: Impact of environmental heterogeneity on the dynamics of a dissipating supercell thunderstorm. *Mon. Wea. Rev.*, **143**, 4244–4277, https://doi.org/10.1175/MWR-D-15-0072.1.

——, C. L. Ziegler, and M. I. Biggerstaff, 2019: Creating a more realistic idealized supercell thunderstorm evolution via incorporation of base-state environmental variability. *Mon. Wea. Rev.*, **147**, 4177–4198, https://doi.org/10.1175/MWR-D-18-0447.1.

Deardorff, J. W., 1980: Stratocumulus-capped mixed layers derived from a three-dimensional model. *Bound.-Layer Meteor.*, **18**, 495–527, https://doi.org/10.1007/BF00119502.

Doyle, J. D., and Q. Jiang, 2006: Observations and numerical simulations of mountain waves in the presence of directional wind shear. *Quart. J. Roy. Meteor. Soc.*, **132**, 1877–1905, https://doi.org/10.1256/qj.05.140.

Frame, J., and P. Markowski, 2006: The interaction of simulated squall lines with idealized mountain ridges. *Mon. Wea. Rev.*, **134**, 1919–1941, https://doi.org/10.1175/MWR3157.1.

Hannesen, R., N. Dotzek, H. Gysi, and K. D. Beheng, 1998: Case study of a tornado in the upper Rhine Valley. *Meteor. Z.*, **7**, 163–170, https://doi.org/10.1127/metz/7/1998/163.

Homar, V., M. Gayà, R. Romero, C. Ramis, and S. Alonso, 2003: Tornadoes over complex terrain: An analysis of the 28th August 1999 tornadic event in eastern Spain. *Atmos. Res.*, **67–68**, 301–317, https://doi.org/10.1016/S0169-8095(03)00064-4.

Hunt, J. C., K. J. Richards, and P. W. M. Brighton, 1988: Stably stratified shear flow over low hills. *Quart. J. Roy. Meteor. Soc.*, **114**, 859–886, https://doi.org/10.1002/qj.49711448203.

Jiang, G.-S., and C.-W. Shu, 1996: Efficient implementation of weighted ENO schemes. *J. Comput. Phys.*, **126**, 202–228, https://doi.org/10.1006/jcph.1996.0130.

Katona, B., P. Markowski, C. Alexander, and S. Benjamin, 2016: The influence of topography on convective environments in the eastern United States as deduced from HRRR output. *Wea. Forecasting*, **31**, 1481–1490, https://doi.org/10.1175/WAF-D-16-0038.1.

Kirshbaum, D. J., F. Fabry, and Q. Cazenave, 2016: The Mississippi Valley convection minimum on summer afternoons: Observations and numerical simulations. *Mon. Wea. Rev.*, **144**, 263–272, https://doi.org/10.1175/MWR-D-15-0238.1.

Klees, A. M., Y. P. Richardson, P. M. Markowski, C. Weiss, J. M. Wurman, and K. K. Kosiba, 2016: Comparison of the tornadic and nontornadic supercells intercepted by VORTEX2 on 10 June 2010. *Mon. Wea. Rev.*, **144**, 3201–3231, https://doi.org/10.1175/MWR-D-15-0345.1.

Klemp, J. B., and R. B. Wilhelmson, 1978: The simulation of three-dimensional convective storm dynamics. *J. Atmos. Sci.*, **35**, 1070–1096, https://doi.org/10.1175/1520-0469(1978)035<1070:TSOTDC>2.0.CO;2.

Kohonen, T., 2013: Essentials of the self-organizing map. *Neural Network*, **37**, 52–65, https://doi.org/10.1016/j.neunet.2012.09.018.

Kovacs, M., and D. J. Kirshbaum, 2016: Topographic impacts on the spatial distribution of deep convection over southern Quebec. *J. Appl. Meteor. Climatol.*, **55**, 743–762, https://doi.org/10.1175/JAMC-D-15-0239.1.

Krocak, M. J., and H. E. Brooks, 2018: Climatological estimates of hourly tornado probability for the United States. *Wea. Forecasting*, **33**, 59–69, https://doi.org/10.1175/WAF-D-17-0123.1.

LaPenta, K. D., L. F. Bosart, T. J. Galarneau Jr., and M. J. Dickinson, 2005: A multiscale examination of the 31 May 1998 Mechanicville, New York, tornado. *Wea. Forecasting*, **20**, 494–516, https://doi.org/10.1175/WAF875.1.

Letkewicz, C. E., and M. D. Parker, 2010: Forecasting the maintenance of mesoscale convective systems crossing the Appalachian Mountains. *Wea. Forecasting*, **25**, 1179–1195, https://doi.org/10.1175/2010WAF2222379.1.

——, and ——, 2011: Impact of environmental variations on simulated squall lines interacting with terrain. *Mon. Wea. Rev.*, **139**, 3163–3183, https://doi.org/10.1175/2011MWR3635.1.

——, A. J. French, and M. D. Parker, 2013: Base-state substitution: An idealized modeling technique for approximating environmental variability. *Mon. Wea. Rev.*, **141**, 3062–3086, https://doi.org/10.1175/MWR-D-12-00200.1.

Lyza, A. W., and K. R. Knupp, 2018: A background investigation of tornado activity across the southern Cumberland Plateau terrain system of northeastern Alabama. *Mon. Wea. Rev.*, **146**, 4261–4278, https://doi.org/10.1175/MWR-D-18-0300.1.

——, T. A. Murphy, B. T. Goudreau, P. T. Pangle, K. R. Knupp, and R. A. Wade, 2020: Observed near-storm environment variations across the southern Cumberland Plateau system in northeastern Alabama. *Mon. Wea. Rev.*, **148**, 1465–1482, https://doi.org/10.1175/MWR-D-19-0190.1.

Markowski, P., and Y. Richardson, 2006: On the classification of vertical wind shear as directional shear versus speed shear. *Wea. Forecasting*, **21**, 242–247, https://doi.org/10.1175/WAF897.1.

——, and ——, 2007: Observations of vertical wind shear heterogeneity in convective boundary layers. *Mon. Wea. Rev.*, **135**, 843–861, https://doi.org/10.1175/MWR3334.1.

——, and N. Dotzek, 2011: A numerical study of the effects of orography on supercells. *Atmos. Res.*, **100**, 457–478, https://doi.org/10.1016/j.atmosres.2010.12.027.

——, and Y. P. Richardson, 2014: The influence of environmental low-level shear and cold pools on tornadogenesis: Insights from idealized simulations. *J. Atmos. Sci.*, **71**, 243–275, https://doi.org/10.1175/JAS-D-13-0159.1.

——, J. M. Straka, E. N. Rasmussen, and D. O. Blanchard, 1998: Variability of storm-relative helicity during VORTEX. *Mon. Wea. Rev.*, **126**, 2959–2971, https://doi.org/10.1175/1520-0493(1998)126<2959:VOSRHD>2.0.CO;2.

Murray, J. C., and B. A. Colle, 2011: The spatial and temporal variability of convective storms over the northeast United States during the warm season. *Mon. Wea. Rev.*, **139**, 992–1012, https://doi.org/10.1175/2010MWR3316.1.

Nowotarski, C., and A. Jensen, 2013: Classifying proximity soundings with self-organizing maps toward improving supercell and tornado forecasting. *Wea. Forecasting*, **28**, 783–801, https://doi.org/10.1175/WAF-D-12-00125.1.

Panosetti, D., S. Böing, L. Schlemmer, and J. Schmidli, 2016: Idealized large-eddy and convection-resolving simulations of moist convection over mountainous terrain. *J. Atmos. Sci.*, **73**, 4021–4041, https://doi.org/10.1175/JAS-D-15-0341.1.

Reeves, H. D., and Y.-L. Lin, 2007: The effects of a mountain on the propagation of a preexisting convective system for blocked and unblocked flow regimes. *J. Atmos. Sci.*, **64**, 2401–2421, https://doi.org/10.1175/JAS3959.1.

Richardson, Y. P., K. K. Droegemeier, and R. P. Davies-Jones, 2016: The influence of horizontal environmental variability on numerically simulated convective storms. Part I: Variations in vertical shear. *Mon. Wea. Rev.*, **135**, 3429–3455, https://doi.org/10.1175/MWR3463.1.

Schneider, D. G., 2009: The impact of terrain on three cases of tornadogenesis in the Great Tennessee Valley. *Electron. J. Oper. Meteor.*, **10**, 1–33.

Sherburn, K. D., and M. D. Parker, 2014: Climatology and ingredients of significant severe convection in high-shear, low-CAPE environments. *Wea. Forecasting*, **29**, 854–877, https://doi.org/10.1175/WAF-D-13-00041.1.

Smith, T. L., S. G. Benjamin, J. M. Brown, S. Weygandt, T. Smirnova, and B. Schwartz, 2008: Convection forecasts from the hourly updated, 3-km High Resolution Rapid Refresh (HRRR) model. *24th Conf. on Severe Local Storms*, Savannah, GA, Amer. Meteor. Soc., 11.1, https://ams.confex.com/ams/pdfpapers/142055.pdf.

Soderholm, B., B. Ronalds, and D. J. Kirshbaum, 2014: The evolution of convective storms initiated by an isolated mountain ridge. *Mon. Wea. Rev.*, **142**, 1430–1451, https://doi.org/10.1175/MWR-D-13-00280.1.

Tang, B., M. Vaughn, R. L. Azear, K. Corbosiero, L. Bosart, T. Wasula, I. Lee, and K. Tipton, 2016: Topographic and boundary influences on the 22 May 2014 Duanesburg, New York, tornadic supercell. *Wea. Forecasting*, **31**, 107–127, https://doi.org/10.1175/WAF-D-15-0101.1.

Teng, J.-H., C.-S. Chen, T.-C. C. Wang, and Y.-L. Chen, 2000: Orographic effects on a squall line system over Taiwan. *Mon. Wea. Rev.*, **128**, 1123–1138, https://doi.org/10.1175/1520-0493(2000)128<1123:OEOASL>2.0.CO;2.

Thompson, R. L., R. Edwards, J. A. Hart, K. L. Elmore, and P. M. Markowski, 2003: Close proximity soundings within supercell environments obtained from the Rapid Update Cycle. *Wea. Forecasting*, **18**, 1243–1261, https://doi.org/10.1175/1520-0434(2003)018<1243:CPSWSE>2.0.CO;2.

——, B. T. Smith, J. S. Grams, A. R. Dean, and C. Broyles, 2012: Convective modes for significant severe thunderstorms in the contiguous United States. Part II: Supercell and QLCS tornado environments. *Wea. Forecasting*, **27**, 1136–1154, https://doi.org/10.1175/WAF-D-11-00116.1.

Vosper, S. B., S. D. Mobbs, and B. A. Gardiner, 2002: Measurements of the near-surface flow over a hill. *Quart. J. Roy. Meteor. Soc.*, **128**, 2257–2280, https://doi.org/10.1256/qj.01.11.

Weckwerth, T. M., L. J. Bennett, L. J. Miller, J. V. Baelen, P. D. Girolamo, A. M. Blyth, and T. J. Hertneky, 2014: An observational and modeling study of the processes leading to deep, moist convection in complex terrain. *Mon. Wea. Rev.*, **142**, 2687–2708, https://doi.org/10.1175/MWR-D-13-00216.1.

Wunsch, M. S., and M. M. French, 2020: Delayed tornadogenesis within New York State severe storms. *J. Oper. Meteor.*, **8**, 79–92, https://doi.org/10.15191/nwajom.2020.0806.